ADVANCES IN GEOPHYSICS, VOL. 37

POROELASTIC TECHNIQUES IN THE STUDY OF EARTHQUAKE-RELATED HYDROLOGIC PHENOMENA

EVELYN ROELOFFS
U.S. Geological Survey
5400 MacArthur Blvd.
Vancouver, Washington 98661

1. INTRODUCTION

Earthquakes cause a variety of hydrologic phenomena, including changes in groundwater levels, streamflow and spring discharges, and rapid well level fluctuations resembling seismograms. Some of these changes can be explained by poroelastic response to the earthquake's strain field, but others seem to reflect nonelastic processes such as changes in permeability near the earthquake's rupture zone (e.g., Rojstaczer and Wolf, 1992). Seismic water level oscillations continue to be observed but the degree to which they match theory (Cooper *et al.*, 1965; Liu *et al.*, 1989) bears further investigation. Observations have also been made of water level changes caused by fault creep (e.g., Roeloffs *et al.*, 1989).

Subsurface fluid pressure, p, affects the frictional resistance, τ, of faults according to the effective stress law combined with the Coulomb failure criterion (e.g., Scholz, 1990):

$$\tau = \mu(-\sigma_n - p), \tag{1}$$

where μ is the coefficient of friction and σ_n is normal stress across the fault plane (extension positive). There is now compelling evidence that τ on the San Andreas fault zone is low, on the order of 10 MPa (Zoback *et al.*, 1987), and high pore fluid pressure is an attractive explanation. There is still debate, however, as to whether natural earthquakes are initiated by increasing p, decreasing μ, or increasing tectonic shear stress. Earthquakes artificially induced by reservoir impoundment (e.g., Roeloffs, 1988a) or fluid injection (e.g., Hsieh and Bredehoeft, 1981) are almost certainly attributable to increased pore pressure. Fluid extraction from the subsurface also triggers earthquakes; Segall (1989, 1992) has shown that poroelastic contraction of the zone from which the fluids are produced can destablize faults by changing shear and normal stress at locations where fluid mass content does not change. Poroelastic models predict that reservoir impoundment and fluid extraction affect τ by only a small

amount, on the order of 0.1 MPa or less. Many question whether changes in τ so small compared with earthquake stress drops can explain induced earthquakes. On the other hand, some investigators contend that even natural variations in the groundwater recharge rate influence seismicity (e.g., Costain *et al.*, 1987; Roth *et al.*, 1992).

Hydrologic changes preceding earthquakes continue to be reported, and the documentation of a few of these reports is now approaching levels that require them to be given scientific credibility. Advances in understanding hydrologic responses to tectonic stress and strain facilitate the investigation of reported hydrologic precursors.

This article describes examples of the phenomena just listed and summarizes poroelastic methods currently available for their interpretation. In particular, it has been shown that well water levels can be used to measure tectonic strain over a limited frequency band that depends critically on the degree of aquifer confinement (e.g., Rojstaczer, 1988b). Although chemistry plays an important role in earthquake hydrology, only mechanical and fluid–dynamic effects can be modeled using poroelasticity. Hypotheses regarding the role of fluids in generating natural earthquakes are largely outside the scope of this article, because few observations are available to constrain them. Instead, the emphasis is on hydrologic data related to earthquakes and their quantitative interpretation.

2. Examples of Earthquake-Related Hydrologic Phenomena

A number of earthquakes (Table 1) provide examples of earthquake-related hydrologic effects, either because those effects were remarkable or because they were well documented. The examples are summarized in chronological order to familiarize the reader with the variety of phenomena to be considered. Some of these observations are analyzed quantitatively in later sections, but others remain unexplained.

The 1964 Alaska Earthquake (M_s 8.6)

The M_s 8.6 Alaska earthquake of 1964 produced water level fluctuation in more than 600 wells throughout the United States and Puerto Rico (Waller *et al.*, 1965). Coble (1967) gives a detailed description of water level changes in the state of Iowa, which included not only seismic oscillations and turbidity, but also water level rises of as much as 16 m that persisted for months. Scott and Render (1964) recorded a water level drop

TABLE 1. EXAMPLES OF EARTHQUAKE-RELATED HYDROLOGIC PHENOMENA

Location and date (UT)	Magnitude (M_s)	Focal mechanism	Phenomena	References
Alaska, USA March 28, 1964	8.6	Thrust faulting	Seismic oscillations Groundwater changes in midwestern United States and Canada	Coble, 1967 Scott and Render, 1964 Bower and Heaton, 1978
Haicheng, China February 4, 1975	7.4	Left-lateral strike-slip	Water level anomalies began about 3 months before the earthquake	Deng *et al.*, 1981 Zhu and Zhong, 1979 Ma *et al.*, 1989
Tangshan, China July 27, 1976	7.6	Right-lateral strike-slip M7.1 oblique thrust aftershock 15 hours later	Water level anomalies began as early as 4 years before the earthquake	Wang *et al.*, 1979 Wu *et al.*, 1984 Zhang and Qiou, 1979 Ma *et al.*, 1989
Borah Peak, Idaho, USA October 28, 1983	7.3	Normal faulting	Groundwater discharge after the earthquake	Whitehead *et al.*, 1984/85 1984/85
Kettleman Hills, California, USA August 4, 1985	5.8	Thrust faulting	Coseismic water level drops Possible precursor	Ekstrom *et al.*, 1992 Roeloffs and Quilty, 1995
Loma Prieta, California, USA October 18, 1989	7.1	Right-lateral strike-slip and reverse	Discharge increase and well level decrease Possible precursors	Rojstaczer and Wolf, 1992 Roeloffs, 1993
Landers, California June 28, 1992	7.4	Right-lateral strike-slip	Remote triggered seismicity	Hill *et al.*, 1993 Roeloffs *et al.*, 1994

in a well near Ottowa, Canada (Fig. 1). This 28-cm drop took place over about an hour, but persisted for several days. Bower and Heaton (1978) were able to show that the form of this response matched the expected response to an extensional volumetric strain of about 3×10^{-7}, but could not explain how the passage of seismic waves could produce strain of that magnitude.

The 1975 Haicheng, China, Earthquake (M_s 7.4)

The Haicheng earthquake is the single instance in which an early warning enabled hundreds of thousands of people to evacuate unsafe buildings. A vigorous and ominously intensifying foreshock sequence prompted the warning, but more than 240 groundwater anomalies also were reported in the three months preceding the event (Deng *et al.*, 1981; Zhu and Zhong, 1979).

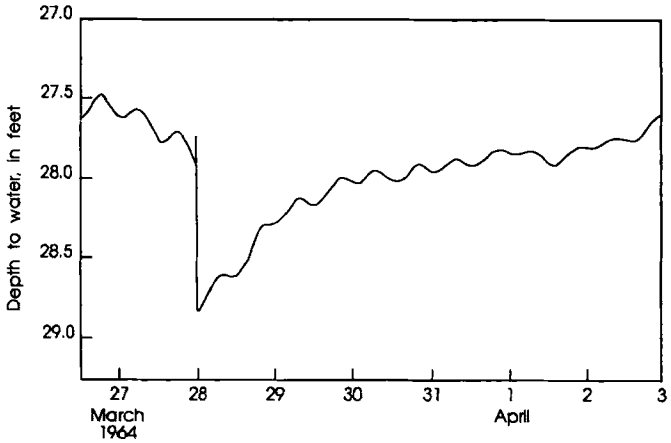

FIG. 1. Water level recorded in a well near Ottawa, Canada, at the time of the 1964 Alaska earthquake (Scott and Render, 1964).

The 1976 Tangshan, China, Earthquake (M_s 7.6)

There is still controversy about the significance of electromagnetic, geodetic, and hydrologic anomalies that occurred before this intraplate earthquake that leveled the city of Tangshan, killing as many as half a million people. Well levels in Tangshan, Tianjin, and Beijing began to decline as early as four years beforehand (Figs. 2a and b). Wang *et al.* (1979) argue that these changes cannot be accounted for by groundwater withdrawal. leaving open the possibility that they were precursors to the Tangshan earthquake.

The 1983 Borah Peak, Idaho, Earthquake (M_s 7.3)

This normal faulting event greatly increased river base flows and other groundwater discharge, especially from carbonate springs. Major rivers in the area experienced significantly increased flow for about six months following the earthquake (Whitehead *et al.*, 1984/85; Wood, 1985).

The 1985 Kettleman Hills, California, Earthquake (M_s 5.8)

Steplike coseismic water level drops were recorded at four wells near Parkfield, California, that had been instrumented as part of the Parkfield, California, earthquake prediction experiment (Figs. 3a and b) (Ekstrom *et al.*, 1992; Roeloffs and Quilty, 1995). Further scrutiny of these records

revealed small changes in water level beginning three days before the earthquake in two of the wells, as well as a compressional signal on one borehole strainmeter (Roeloffs and Quilty, 1995). The water level rise was shown to be unique in more than five years of data from one of the wells, and it was possible to show that one of the wells that did not record the anomaly could not have recorded it because the aquifer it samples is too poorly confined. The significance of these phenomena as earthquake precursors is open to question because the signal was not recorded at the fourth well or at two other borehole strainmeters.

The 1989 Loma Prieta, California, Earthquake (M_s 7.1)

The Loma Prieta earthquake, a $M_s = 7.1$ event with both strike-slip and thrust displacement, was followed by increased discharge in streams draining the rupture zone. Rojstaczer and Wolf (1992) investigated these changes and discovered that groundwater levels had dropped in the ridges where these streams originated, an observation less obvious than the streamflow increases. Stream water chemistry after the earthquake was consistent with an increased flow of groundwater into the streams, leading Rojstaczer and Wolf to conclude that the earthquake temporarily raised permeability of aquifers and aquitards near the rupture zone.

A citizen hiking at the time of the earthquake reported an increase in discharge over a waterfall about an hour before the earthquake; a follow-up investigation confirmed postseismic increased discharge at that location and showed that a significant part of the increased discharge must have derived from a single spring about 1 km upstream of the waterfall (Roeloffs, 1993).

The 1992 Landers, California Earthquake (M_s 7.4)

The most remarkable aspect of the Landers earthquake is its triggering of seismic activity at locations as far as several hundred kilometers from the epicenter (Hill *et al.*, 1993). Postseismic hydrologic effects in southern California include gas bubbling, increased spring discharge, and groundwater level changes. At distances of 400 to 1100 km, water level oscillations were recorded, some followed by persistent offsets (Roeloffs *et al.*, 1995).

In addition to these examples, Muir-Wood and King (1993) describe earthquake aftereffects, and Roeloffs (1988b) describes other reports of hydrologic earthquake precursors. The rest of this article emphasizes poroelastic techniques that can be used to analyze such phenomena quantitatively.

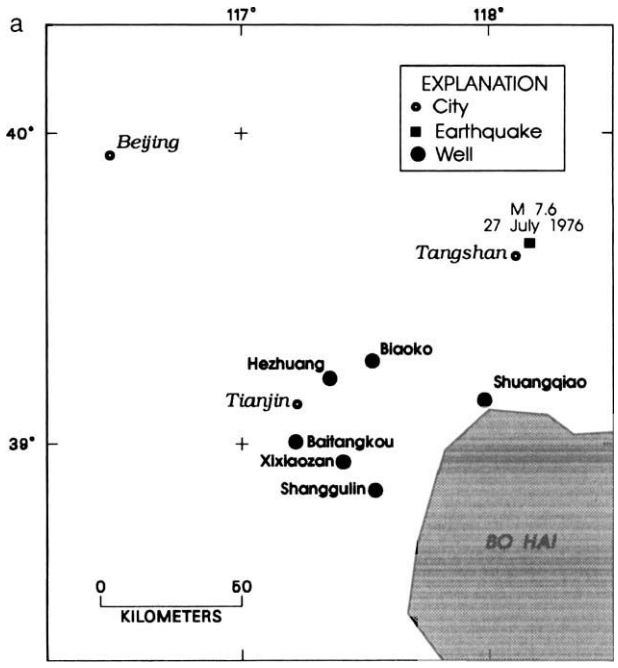

FIG. 2. (a) Location map showing the epicenter of the 1976 Tangshan, China, main shock and the locations of water wells monitored near Tianjin. (Wu *et al.*, 1984.) (b) Water levels, in meters, from the wells shown in part a. The well depths are given in parentheses after each well's name (Wu *et al.*, 1984). (Reproduced with permission.)

3. Stress, Strain, Fluid Pressure, and Fluid Mass Content

3.1. Poroelastic Constitutive Relations

The stress–strain (or constitutive) relations for an ordinary isotropic, linearly elastic solid can be expressed as:

$$2G\epsilon_{ij} = \sigma_{ij} - \frac{\nu}{(1+\nu)}\sigma_{kk}\delta_{ij}, \tag{2}$$

where ϵ_{ij} is the dimensionless strain tensor; σ_{ij} is the stress tensor, which has dimensions of force per unit area; δ_{ij} is the Kronecker delta; and the summation convention is implied. The subscripts range through the coordinate directions x, y, and z. The material is characterized by G, the shear modulus (force per unit area) and ν, the Poisson ratio (dimensionless).

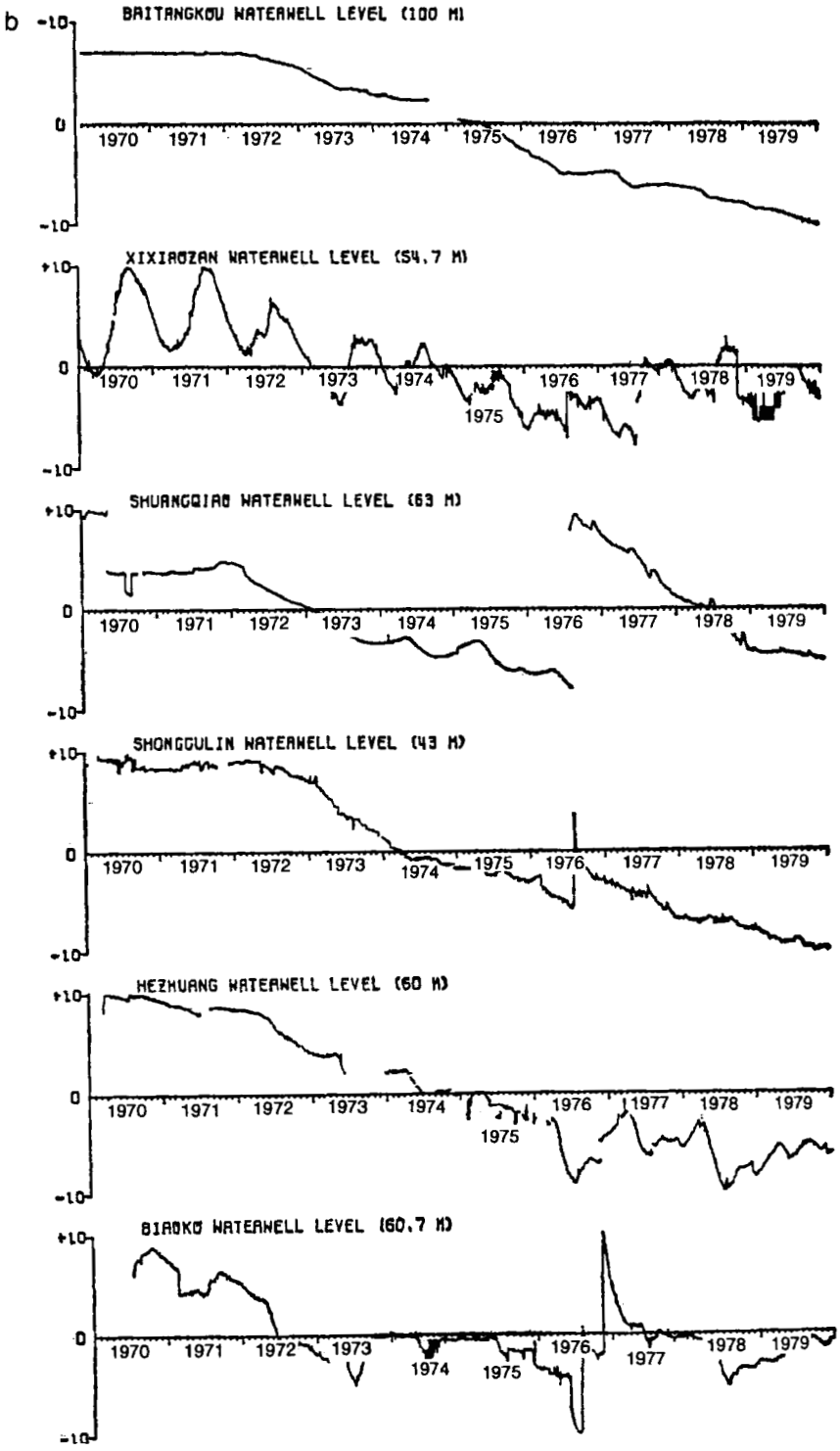
b
BAITANGKOU WATERWELL LEVEL (100 M)
XIXIAOZAN WATERWELL LEVEL (54.7 M)
SHUANGQIAO WATERWELL LEVEL (63 M)
SHONGGULIN WATERWELL LEVEL (43 M)
HEZHUANG WATERWELL LEVEL (60 M)
BIAOKO WATERWELL LEVEL (60.7 M)
+10
0
-10
1970
1971
1972
1973
1974
1975
1976
1977
1978
1979

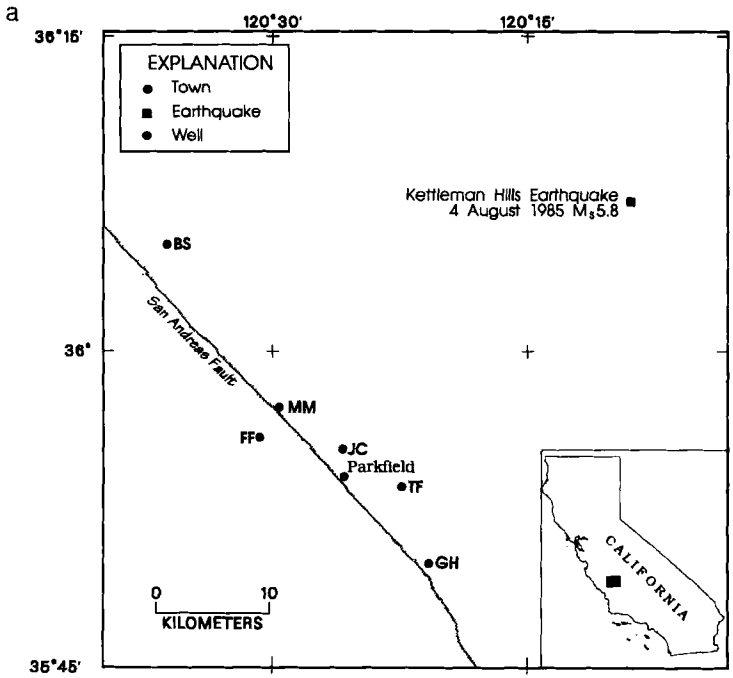

FIG. 3. (a) Map showing the locations of wells near Parkfield, California, monitored as part of the Parkfield earthquake prediction experiment.

The diagram in Fig. 4 shows the coordinate system and stress components; extension is taken to be positive.

Elastic strain is generally small and will be expressed here in microstrain (part per million) or nanostrain (part per billion). In the earth's crust, the absolute magnitudes of the stress and strain tensor components are usually unknown, and may be too large to be modeled using linear elasticity. Equation (2) is applicable when the stress and strain tensors are interpreted as changes relative to a reference state, and this meaning will be attributed to these quantities throughout this article.

For intact rocks, a shear modulus within an order of magnitude of 3×10^4 megapascals (MPa) is typical; liquids have a shear modulus of zero. The Poisson ratio is always greater than -1 and reaches a maximum of $1/2$ for liquids or incompressible materials; for rocks, typical values are between 0.2 and 0.4.

There are many other choices of the two material properties characterizing the behavior of an isotropic linearly elastic solid. The bulk modulus, K,

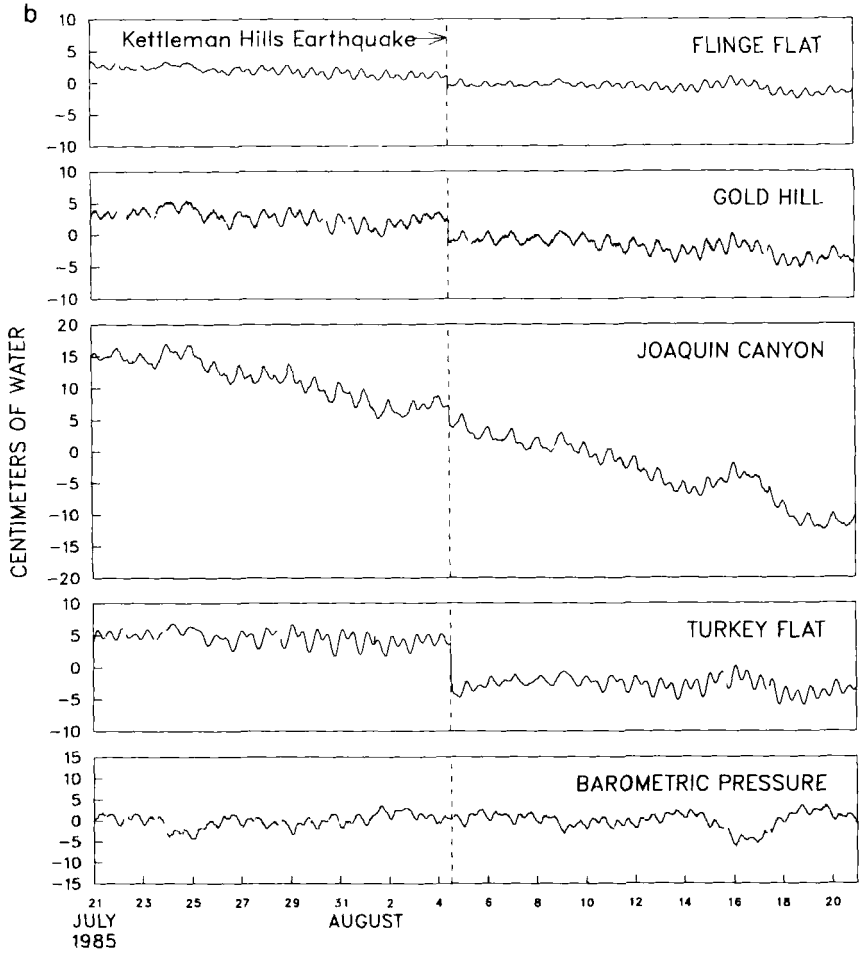

FIG. 3. (b) Raw water level data from wells in Parkfield for a month centered on the time of the Kettleman Hills earthquake. The earthquake had a magnitude of 5.8 and occurred about 35 km from the wells. The raw data show earth tide and barometric effects, as well as water level drops at the time of the earthquake.

given by

$$K = 2G(1 + \nu)/[3(1 - 2\nu)], \tag{3}$$

will also be used here. The compressibility is the reciprocal of the bulk modulus.

For an isotropic, linearly elastic, porous medium, the stress-strain relations (2) must be augmented to incorporate the effect of fluid pressure.

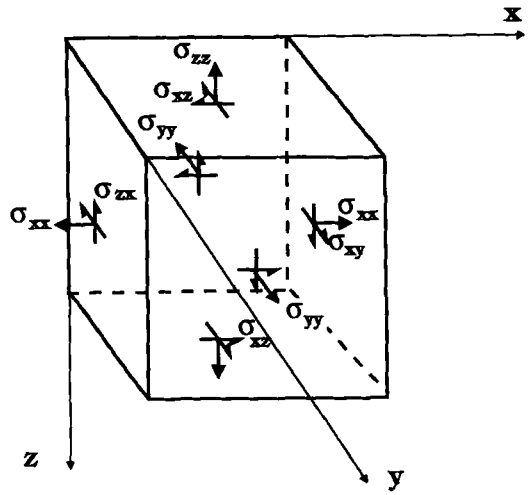

FIG. 4. Coordinate system and stress tensor components. The coordinate system is right-handed with z downward. Extension is positive; compression is negative. The same conventions are used for the strain components.

Biot (1941) was the first to accomplish this in a general formulation; Biot (1956) and Biot and Willis (1957) presented the poroelastic constitutive relations in a variety of forms whose advantages and disadvantages were recently summarized by Wang (1993). Here the development chosen is that of Rice and Cleary (1976), who augmented (2) by the addition of pore pressure as a variable on the stress side of the equations, and fluid mass content per unit volume, m, on the strain side, resulting in the following constitutive relations:

$$2G\epsilon_{ij} = \sigma_{ij} - \frac{\nu}{(1+\nu)}\sigma_{kk}\delta_{ij} + \frac{3(\nu_u - \nu)}{B(1+\nu)(1+\nu_u)}p\delta_{ij}, \tag{4a}$$

$$m - m_0 = \frac{3\rho_0(\nu_u - \nu)}{2GB(1+\nu)(1+\nu_u)}\left(\sigma_{kk} + \frac{3}{B}p\right), \tag{4b}$$

where m_0 and ρ_0 are the fluid mass content and density, and m_0, ρ_0, and p are all interpreted as measurements with respect to the same reference state used for the stress and strain tensors. The term ν_u represents the "undrained" Poisson ratio, and B is called Skempton's coefficient. The

examples described in the next sections will clarify the meanings of these material properties.

3.2. Pore Pressure Buildup in Undrained Compression

"Drained" conditions are idealized conditions under which there is no change in fluid pressure, while "undrained" conditions are those in which there is no fluid flow. (Mathematically, they correspond to the isothermal and adiabatic conditions of linear thermoelasticity, e.g., Boley and Wiener, 1960). Under either set of conditions, the relationship between stress and strain for the fluid-infiltrated poroelastic material is indistinguishable from that of an ordinary elastic material, provided the correct pair of coefficients is used: G and ν for drained situations, and G and ν_u for undrained situations. The same shear modulus applies over the entire range from drained to undrained conditions. The undrained Poisson ratio is always larger than the drained Poisson ratio, but must be smaller than $1/2$.

The mathematical definition of "undrained" conditions is that $m - m_0 = 0$. The definition of "drained" conditions is that $p = 0$, meaning that there is no change in p from a reference state.

Drained and undrained conditions received their names because of laboratory tests that duplicate these respective conditions. Although these limiting cases can never be achieved exactly in nature, they are closely approached in some situations. Natural examples of undrained deformation include the instantaneous response of groundwater levels to the static strain field of an earthquake, or the response of confined aquifer water pressure to earth tides. In the first case, deformation is undrained because it occurs too rapidly for flow to take place. In the second case, deformation is undrained because the driving force has a large spatial extent; thus pore pressure gradients are small and induce negligible flow.

The increase in pore pressure that results when a porous medium is compressed without allowing fluid to escape is arguably the most important poroelastic phenomenon (Fig. 5). Setting $m = m_0$ in Eq. (4b) yields

$$p = -B\sigma_{kk}/3, \tag{5a}$$

which shows that under undrained conditions, there is a change in fluid pressure proportional to the change in mean stress. The magnitude of the change is governed by Skempton's coefficient, B, which is always between 0 and 1. Thus the maximum pore pressure change that can be produced is equal to the change in mean stress. This bound is not necessarily valid for a medium in which fluid occupies an isolated fracture. The change in fluid

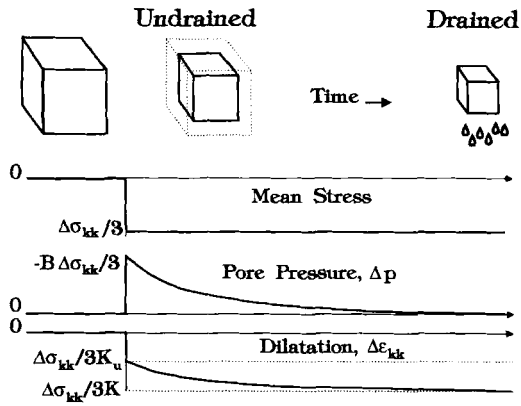

FIG. 5. Diagram illustrating the behavior of a porous elastic material subjected to an increment of mean stress having a step-function time history. Initial contraction of the material is governed by the undrained bulk modulus, K_u, and is accompanied by an increase of pore pressure. This pore pressure will decay if fluid is free to leave the material, and as fluid drains, additional contraction will take place, with final deformation governed by the drained bulk modulus, K.

pressure in the fracture is equal to the change of normal stress perpendicular to the fracture and can consequently exceed the mean stress change.

Equation (5a) can be recast to relate pore pressure change to volumetric strain, ϵ_{kk}:

$$p = -\frac{2GB}{3}\frac{1+\nu_u}{1-2\nu_u}\epsilon_{kk}. \tag{5b}$$

Typical values of the coefficient on the right side of (5b) are 5 to 50 GPa, or 0.5 to 5.0×10^6 m of water. For example, if this coefficient equals 10 GPa, then compressive strain of 10^{-6} (1 part per million, or ppm) can produce a pressure rise of 0.01 MPa, or 1 m of water.

No fluid flow is required to produce the pore pressure increase given by (5a) or (5b). Consequently, pore pressure changes simultaneously with mean stress or volumetric strain. The material's permeability or diffusivity has no effect on the time scale with which such pore pressure changes occur. Equations (5a) and (5b) also imply that in a uniform, isotropic porous elastic medium, no pore pressure change is expected from deformation that produces only shear stress or strain.

3.3. Calculating and Measuring the Poroelastic Constants

For unconsolidated materials, it is reasonable to assume that the bulk medium is much more compressible than either the pore fluid or the solid grains in the medium. When the pore fluid and grains are assumed to be incompressible, $\nu_u = 0.5$ and $B = 1$. Because soil mechanics problems are appropriately dealt with this way, there are many mathematical solutions in the literature for porous media with incompressible constituents, often described as "consolidation" problems. Unfortunately, this assumption is not reasonable for most rocks, and the appropriate formulation to use is that for compressible constituents.

There are few measurements of ν_u, and B has been measured only at low pressures. Furthermore, although ν_u and B have straightforward physical interpretations, they are not independent of each other. For example, as B decreases, the largest possible difference between ν_u and ν must also decrease. Representative values for B and ν_u can be estimated using the following relationships from Rice and Cleary (1976):

$$B = \frac{1/K - 1/K_s}{v_0(1/K_f - 1/K_s) + (1/K - 1/K_s)}, \tag{6}$$

$$\nu_u = \frac{3\nu + B(1 - 2\nu)(1 - K/K_s)}{3 - B(1 - 2\nu)(1 - K/K_s)}, \tag{7}$$

where v_0 is the fluid volume fraction in the reference state (essentially equal to the porosity), K_f is the fluid bulk modulus, K_s is the bulk modulus of the solid grains in the rock, and K is the bulk modulus of the saturated rock under drained conditions. An undrained bulk modulus, K_u can be defined by substituting ν_u for ν in Eq. (3).

Equations (6) and (7) are simplifications of expressions (4) and (6) of Rice and Cleary (1976) that are appropriate when the porosity forms a continuous network and when the grains are all of the same isotropic material. It is usually reasonable to assume that K is equal to the bulk modulus of the dry rock. With all these assumptions in force, laboratory measurements of elastic properties and porosity can be used to estimate the poroelastic properties B and ν_u. Green and Wang (1986) found that poroelastic properties estimated in this way were close to measured values, while Mesri *et al.* (1976) found that the calculated values of B were somewhat too high.

Mesri *et al.* (1976) measured B for a sandstone, a limestone, a marble, and a granite and found that for all four rock types, B was close to 1 at

low effective pressures, but fell to values between 0.33 and 0.69 at effective pressures of 10 MPa. Green and Wang (1986) determined B for three sandstones and a dolomite, and also found values close to 1 at zero effective pressure, but lower values at higher effective pressures. Beavan *et al.* (1991) estimated values for B from a combination of laboratory measurements on core and well level tidal admittance studies for sandstones of the Nubia formation in Egypt; these values ranged from 0.52 to 0.58.

The effects of undrained pore pressure buildup can be important in laboratory experiments other than those designed to measure B. Blanpied *et al.* (1992) observed undrained fluid pressure buildup in an artificial gouge layer during laboratory tests on granite samples. The pressure buildup, which they attributed partly to gouge compaction, caused a rapid loss of the sample's frictional strength in accordance with (1). Blanpied *et al.* hypothesized that a similar mechanism could lead to earthquake instabilities on natural faults.

3.4. Barometric Response of Confined Aquifers

The poroelastic constitutive relations can be used to explain the fluctuations due to barometric pressure typically observed in continuous water level records (e.g., Fig. 3b). Fluctuations caused by barometric pressure can mask small water level signals of tectonic origin, and the response to barometric pressure reveals some characteristics of the behavior of the well as a strainmeter at periods of one to several days.

Consider a confined poroelastic aquifer of infinite areal extent. Let h be the head in the aquifer, that is, the elevation of the water surface in a piezometer that is open, or screened, to the aquifer (Fig. 6). If the piezometer water level is in equilibrium with the aquifer pore pressure, then a change, Δh, is related to a change in aquifer pore pressure, Δp, by

$$\Delta p = (\rho g)\, \Delta h,$$

where ρ is the density of water and g is the acceleration due to gravity.

Let Δb represent a small increment of barometric pressure, with an increase of pressure being positive. For an aquifer near the earth's surface, there is a resulting increment of vertical compressive stress, i.e.,

$$\Delta \sigma_{zz} = -\Delta b.$$

It is usually reasonable to assume that the barometric pressure is uniform over a large area, in which case it will not induce horizontal expansion or

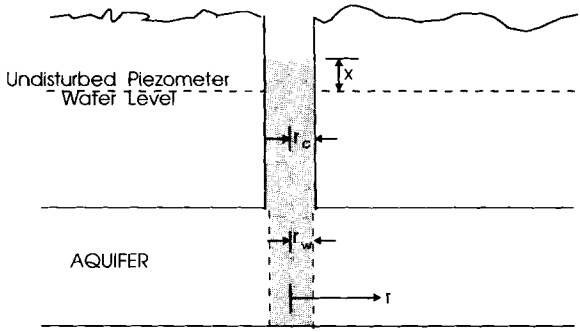

FIG. 6. Diagram illustrating an idealized well in a confined aquifer.

contraction of the aquifer, and there will be no horizontal pressure gradients to induce fluid movement. Mathematically, these conditions correspond to $\epsilon_{xx} = \epsilon_{yy} = 0$, and $m - m_0 = 0$; substitution into the poroelastic constitutive relations (4a and b) expresses the ratio of pore pressure change to barometric pressure change as

$$\frac{\Delta p}{\Delta b} = (B/3)\frac{(1 + \nu_u)}{(1 - \nu_u)} = \alpha. \tag{8}$$

The maximum value of α is 1, achieved when $\nu_u = 0.5$ and $B = 1$. If this pressure is measured in an open piezometer, then an increase in barometric pressure depresses the water level in the piezometer by the same amount. Adding this effect to Eq. (8) yields the barometric response of an open piezometer,

$$\frac{\rho g \Delta h}{\Delta b} = -\left[1 - (B/3)\frac{(1 + \nu_u)}{(1 - \nu_u)}\right] = -(1 - \alpha) = E_B. \tag{9}$$

Thus for an open piezometer, the net response is always a decrease of piezometer water level for an increase of barometric pressure. The E_B term is referred to as the "static confined" barometric efficiency, following usage coined by Rojstaczer (1988b). It can be estimated by using linear regression between records of water level and barometric pressure, and once known, can be used to remove the effect of barometric pressure. The value of E_B is between 0 and -1, according to Eq. (9), and values throughout this range have been observed.

3.5. Volumetric Strain Response

Suppose a confined aquifer is subjected to a volumetric strain, $\Delta\epsilon_{kk}$. Using (5b) the ratio of head change to volumetric strain will be

$$\frac{\Delta h}{\Delta \epsilon_{kk}} = -\frac{1}{\rho g}\frac{2GB}{3}\frac{1+\nu_u}{1-2\nu_u}. \tag{10}$$

If the strain is applied instantaneously (as a step function), then Eq. (10) gives the instantaneous response of the head in the aquifer. In a perfectly confined aquifer compressed over an infinite area, the head will remain at the elevated level indefinitely. If aquifer transmissivity is high enough, then the water level in a piezometer screened in this aquifer will also rise instantaneously by the amount given in Eq. (10). Equation (10) will be referred to as the "static confined volumetric strain efficiency." In practice, however, imperfect aquifer confinement will cause the head increase to bleed off, and the water level change in the piezometer can be either larger or smaller than the static confined response. Modification of the static confined response by these types of flow is described in a Sections 4 and 5.

Water levels in many wells exhibit a nearly static confined response to earth tides. The volumetric strain associated with the solid earth tide is of the order of 10^{-8}, or 10 parts per billion (ppb). Thus if the static confined volumetric strain efficiency is 5×10^6 m of water, earth tides will produce head fluctuations several centimeters in amplitude (e.g., Fig. 3b).

3.6. Tidal Analysis

Equation (10) shows why water level sensors in porous aquifers produce data related to volume strain. Given a record of water level changes caused by earth tides, how does one extract the coefficient in (10)? In principle, once this coefficient is known, the well can be thought of as a calibrated strainmeter. What are the practical limitations of using water wells as strainmeters? In this section, some basic aspects of the solid earth tides are summarized, and it is shown how an analysis of water level tides can be used to evaluate the utility of a well as a strainmeter. Examples of this type of analysis can be found in Narasimhan *et al.* (1984), Hsieh *et al.* (1987), Roeloffs *et al.* (1989), and Beavan *et al.* (1991).

Figure 7 shows water level and borehole strainmeter data from sites near Parkfield, California, together with the equilibrium earth tidal time series calculated for the strainmeter site. The theoretical variation of earth

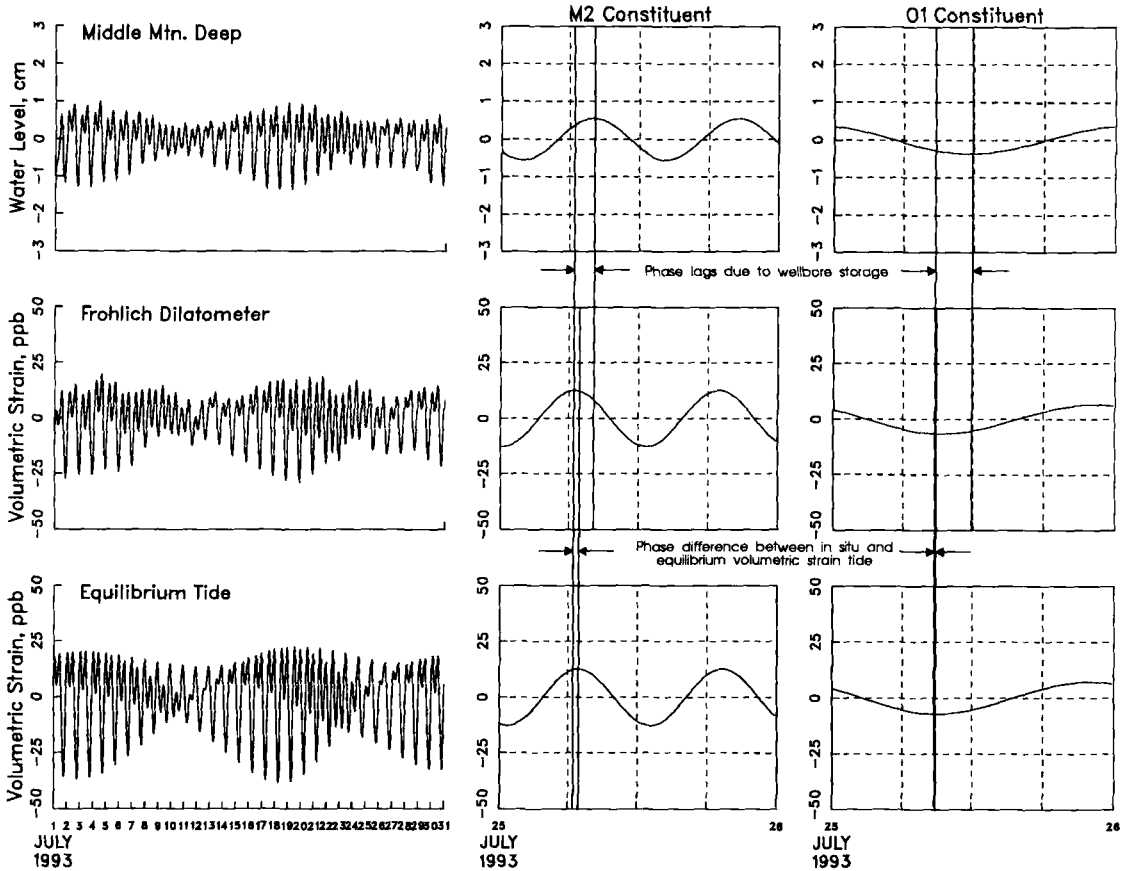

FIG. 7. Graph showing time series of water level, borehole strain, and equilibrium tidal volumetric strain. At the right, the individual M2 and O1 constituents are plotted for each of the time series. The amplitude of the borehole strain data has been expressed in units of strain by equating the amplitude of its M2 constituent to that of the equilibrium tide.

tides with time can be represented exactly by an infinite series of sines and cosines whose fundamental periods are half those of the sun's and moon's revolution about the earth in a geo-centric coordinate system (see, e.g., Godin, 1972). The need for an infinite series arises because the sun's and moon's orbits are complex. However, the tides can be represented by a finite sum to any degree of precision, with the number of terms required increasing with the length of time over which the approximation is required to be valid. Ten to 15 terms are more than sufficient to approximate 30 to 50 days to a precision comparable to hydrograph resolution in the presence of background noise. The periods of the most important constituents and their names are given in Table 2.

A record of well water level or strainmeter data, like the output from a calculation of the equilibrium earth tide, is a single time series that must be broken down into harmonic constituents in order to determine each constituent's amplitude and phase. Over short periods of time (less than about a year), the earth tides do not lend themselves to analysis by Fourier series, in which the constituent frequencies are equally spaced; rather, earth tidal constituents are closely clustered about periods of 12 and 24 hr. Within each of these bands, there are two principal peaks corresponding to the orbital periods of the sun and the moon, respectively. In a finite-length time series, it is easier to estimate accurately the amplitude and phase of the lunar constituents than of the solar constituents, for two reasons. First,

TABLE 2. TIDE CONSTITUENTS APPROPRIATE FOR ANALYSIS OF APPROXIMATELY TWO MONTHS OF WATER LEVEL DATA

Constituent	Period (hours)
Q1	26.86840
O1	25.81930
NO1	24.83320
P1	24.06590
S1	24.00000
K1	23.93450
J1	23.09850
OO1	22.30610
MU2	12.87180
N2	12.65830
M2	12.42060
L2	12.19160
S2	12.00000
K2	11.96720

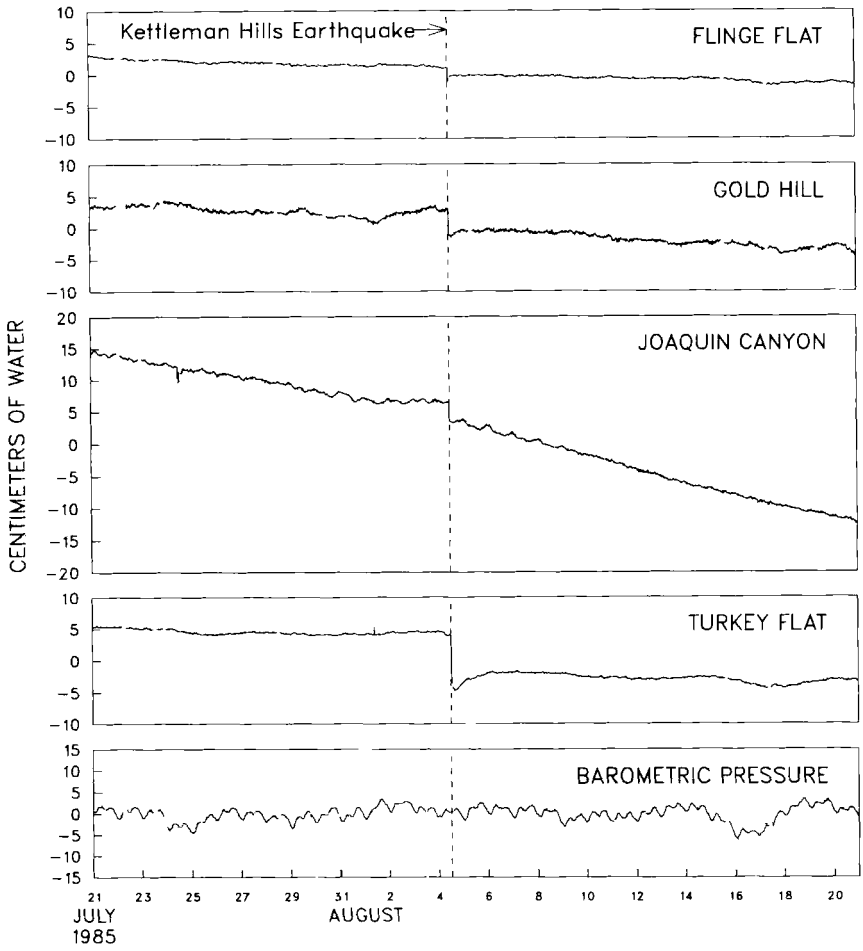

FIG. 8. The water level data from Parkfield at the time of the Kettleman Hills earthquake after removal of earth tide and barometric pressure responses.

the spectrum of the tides happens to be complex at periods near 12.0 and 24.0 hr, with peaks near these periods comprising several large and closely spaced constituents. Second, if temperature and barometric effects are present in the water level data, their strong peaks at 12.0 and 24.0 hr will contaminate the tidal peaks at those periods. Consequently, the most accurately determined constituents are the M2 and O1 terms (the numbers 1 and 2 distinguish tidal constituents with approximately one and two cycles per day, respectively). To separate M2 and O1 from the exactly

semidiurnal and diurnal components, a minimum of 28 days of data is needed.

There are few measurements of the absolute amplitudes of earth tidal strain. Consequently, it must be assumed that theoretically computed tidal strain amplitudes are approximately correct. The tidal gravitational potential induced by the motion of the sun and moon can be calculated with great accuracy (e.g., Harrison, 1971), but the resulting strains are less certain because the elastic structure of the earth is not completely known and because additional strain is induced by the load on the crust due to the oceanic tides. Beaumont and Berger (1975) and Berger and Beaumont (1976) show that even at inland sites, the error due to omitting the ocean loading corrections may be as much as 44% for M2 and that the *in situ* tide is still likely to differ from the ocean load corrected tide by 10%.

For the examples considered here, data are available from borehole strainmeters to provide a reference tidal phase. Borehole strainmeters are not absolutely calibrated instruments; that is, they can be used to determine the phases and relative amplitudes of individual tidal constituents, but not the absolute amplitudes. For many purposes, this limitation is not a problem. In Fig. 7, the strainmeter data have been expressed in ppb by equating the amplitude of the M2 constituent in the strainmeter time series to the amplitude of the same constituent in the equilibrium tide time series. In the example shown, the amplitude ratio of O1 to M2 is 1.03 times larger for the strainmeter than for the equilibrium tide. Ocean loading, heterogeneous material properties, or topographic effects may cause the phase differences, as well as the differences in the amplitude ratios relative to M2, between the strainmeter and the equilibrium tide.

The presence of ocean load effects in the *in situ* tide and of barometric effects in water level and strain data imply that a single coefficient of proportionality between the data and the equilibrium tidal time series will not in general be found. Instead, the M2 and O1 constituents in the data must be isolated and their amplitudes and phases compared with those of the $M2_{eq}$ and $O2_{eq}$ constituents in the equilibrium tide calculated for the same period as the data. The other constituents in Table 2 are routinely analyzed as well, first because larger amplitudes at other periods can diagnose problems with the data, and second because even though these constituents cannot be determined exactly, they can still be subtracted from the data to reveal signals of nontidal origin (Fig. 8).

Once water level and dilatometer data have been processed to extract the M2 and O1 tidal constituents, there will in general be phase differences between these signals, as shown in Fig. 7. These phase differences may be due to flow to the wellbore or to the water table; in addition, a well

tapping a fractured aquifer may exhibit tidal phase lags (Hanson and Owen, 1982; Bower, 1983). The phases can be used to decide which effect is operating and to fit an equation describing how this response varies with frequency. Once the equation is fit, the static confined strain response can be estimated and the response of the well to other strain sources can be predicted. These techniques are described in Sections 4.1 and 6.3.

3.7. Steplike Coseismic Water Level Changes

Within a distance equal to a few source dimensions from its epicenter, an earthquake imposes strain changes that can be viewed as instantaneous strain steps. The coseismic strain field can be calculated if the size and orientation of the earthquake's rupture zone, as well as the amount of slip, are known, using, for example, the programs developed by Okada (1992). According to Eq. (5b), this coseismic strain would be expected to produce steplike water level changes with amplitudes proportional to the volumetric strain field. In particular, water levels should fall in areas that extend, and rise in areas that contract. For example, a quadrantal pattern of rising and falling water levels following the 1974 Izu-Hanto-oki earthquake in Japan was consistent with the volumetric strain field of that strike-slip event (Wakita, 1975). Well level changes accompanying a magnitude 5 earthquake in northeastern Ohio, USA, also rose and fell in locations consistent with the event's focal mechanism (Nicholson *et al.*, 1988).

Where data are available from wells that respond to earth tides, not only the signs, but also the sizes, of the steps can be compared with the earthquake's strain field. As noted earlier, 50 cm/ppm (0.5×10^6 m) is a typical value for the volumetric strain efficiency of a water well, and water levels are usually not measured to better than 1 mm, so that the smallest signal that could be detected would be a strain of 2×10^{-9}, which might be observed 50 km from a magnitude 6 earthquake. Figure 9 shows a contour map of volumetric strain produced by the 1985 Kettleman Hills earthquake, calculated assuming 13 cm of thrust movement on a plane rectangular area extending 20 km along strike and 15 km down-dip. The slip zone is centered at a depth of 13 km and dips 12 deg southwest. The strain at the well sites is between 100 and 200 ppb extension and the static confined strain efficiencies of the wells range from 39 to 54 cm/ppm (Roeloffs and Quilty, 1995), so that the expected step size is 4 to 11 cm. At the Joaquin Canyon, Gold Hill, and Turkey Flat wells, the observed step sizes are 3, 5, and 9 cm, respectively, in good agreement with the expected range. The aquifer sampled by the Flinge Flat well turns out to be very

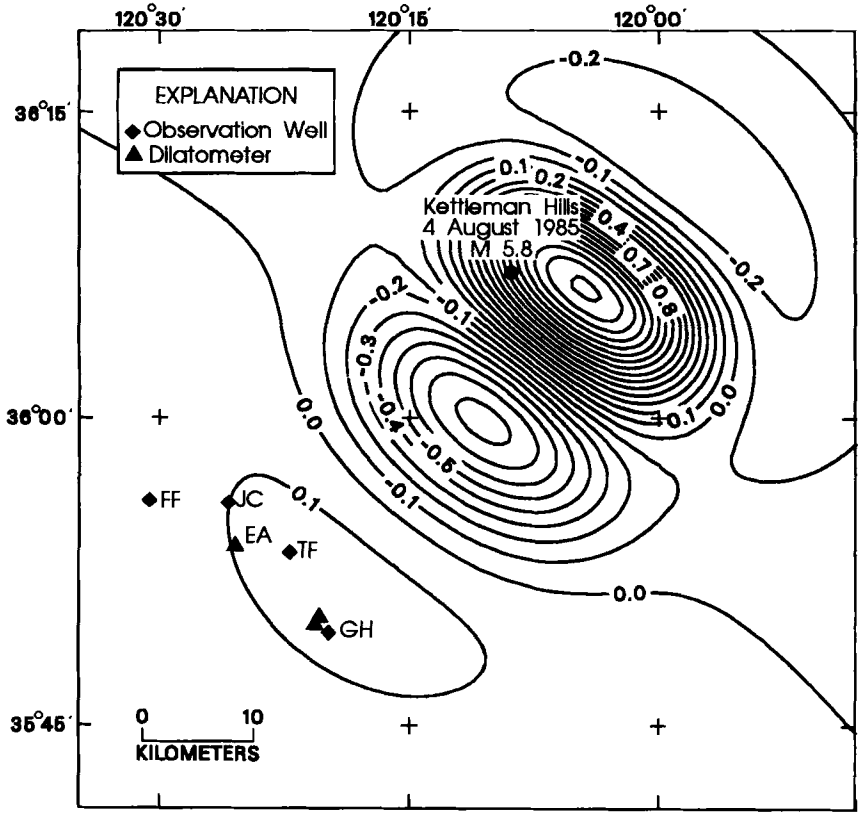

FIG. 9. Contour map of dilatational strain produced by the Kettleman Hills earthquake. Values are in microstrain and extension is positive.

poorly confined, so that the 2-cm water level drop recorded several minutes after the earthquake probably does not reflect the magnitude of the volumetric strain at this location.

4. WELL-AQUIFER SYSTEMS

Well water level is not always exactly equal to aquifer head. If the aquifer transmissivity is relatively low, then well water level changes can be smaller than aquifer head changes and can lag behind them. On the other hand, if aquifer transmissivity is relatively high, then the well–aquifer

system may have a resonant frequency near which the well water level can amplify the aquifer pressure changes by as much as three orders of magnitude.

Evaluation of these effects quantitatively requires us to solve the equations of groundwater flow, but does not require a complete coupling of them to the equations governing deformation. Groundwater flow obeys Darcy's law, which, for a uniform, isotropic medium, is

$$q_i = -\frac{k}{\rho g}\frac{\partial p}{\partial x_i}, \tag{11}$$

where q_i is the rate of fluid volume flow per unit area in the x_i direction and k is hydraulic conductivity (length per unit time). In most hydrogeologic applications, transient groundwater flow is simulated using the diffusion equation

$$\frac{k}{S_s}\nabla^2 p = \frac{\partial p}{\partial t}, \tag{12}$$

where S_s is specific storage (dimensions of length^{-1}), and t is time (e.g., Freeze and Cherry, 1979). The specific storage is defined as the volume of water released from a unit volume of porous aquifer when there is a unit decline of aquifer head. For an aquifer of thickness d, it is often convenient to work with the transmissivity, $T = kd$, and the storativity (or storage coefficient), $S = kS_s$. The rate of diffusion is governed by the hydraulic diffusivity, c, where

$$c = \frac{k}{S_s} = \frac{T}{S}. \tag{13}$$

Aquifer deformation does not appear in Eq. (12), and is not explicitly discussed in most derivations of this equation. An aquifer, however, accommodates (stores) an increment of fluid by a combination of increased pore pressure and aquifer deformation. The diffusion Eq. (12) is valid only for conditions of constant stress in one spatial direction, and zero strain in the two orthogonal directions (Green and Wang, 1990), conditions that are approximated by areally extensive aquifers near the earth's surface.

4.1. Wellbore Storage

"Wellbore storage" is the term used to describe a lag of piezometer water level behind aquifer pressure resulting from the need for water to flow into the borehole in order to equilibrate water level with aquifer

pressure. Wellbore storage effects increase as the transmissivity of the formation decreases. They may be so extreme as to prevent the recording of earth tides in a very tight formation, or they may be negligible at tidal frequencies.

Early work on well response to periodic strain was done by Cooper *et al.* (1965), Bredehoeft (1967), and Bodvarsson (1970). The most general expression for wellbore storage as a function of frequency was developed by Hsieh *et al.* (1987). Assume that aquifer pressure head is varying periodically, with amplitude h_0 and radian frequency ω. The piezometer water level variation w_0 will, in general, have a smaller amplitude and will lag h_0. The equation giving w_0 as a function of frequency, which is obtained by solving (12) with an appropriate boundary condition at the interface between the aquifer and the well casing (Hsieh *et al.*, 1987), can be expressed mathematically as

$$w_0/h_0 = (e + if)^{-1}, \tag{14}$$

where $i = \sqrt{-1}$,

$$e = 1 - \beta[\Psi ker(\alpha_w) + \Phi kei(\alpha_w)], \tag{15a}$$

$$f = \beta[\Phi ker(\alpha_w) - \Psi kei(\alpha_w)], \tag{15b}$$

and

$$\Phi = \frac{-[ker_1(\alpha_w) + kei_1(\alpha_w)]}{2^{1/2}\alpha_w\left[ker_1^2(\alpha_w) + kei_1^2(\alpha_w)\right]}, \tag{16a}$$

$$\Psi = \frac{-[ker_1(\alpha_w) - kei_1(\alpha_w)]}{2^{1/2}\alpha_w\left[ker_1^2(\alpha_w) + kei_1^2(\alpha_w)\right]}. \tag{16b}$$

In (15a and b) and (16a and b), *ker*, *kei*, ker_1, and kei_1 represent Kelvin functions of orders 0 and 1, respectively (Abramowitz and Stegun, 1972), and β and α_w are dimensionless functions of frequency that depend on the well and casing radii and on the reservoir storage coefficient and transmissivity:

$$\alpha_w = (\omega S/T)^{1/2} r_w = (\omega S_s/k)^{1/2} r_w = (\omega c)^{1/2} r_w, \tag{17}$$

$$\beta = \frac{\omega r_c^2}{2T}. \tag{18}$$

In Eqs. (17) and (18), r_w is the radius of the well at the depth where it is open to the aquifer, and r_c is the radius of the well at the depth where the water surface is fluctuating. Also, S is the storage coefficient (dimensionless), and T is the transmissivity. If d is the length of the interval over which the well is open to the aquifer, then $S = dS_s$ and $T = dk$.

When wellbore storage is important at tidal frequencies, M2 and O1 will lag the corresponding constituents in the compressive strain tide, with the lag being greater for M2. The ratio of water level amplitude to strain amplitude will be smaller for M2 than for O1. In Fig. 7, for example, tidal phase lags are caused by wellbore storage. Figure 10 shows how the tidal amplitudes and phases depend on hydraulic conductivity for a typical well geometry and three values of the storage coefficient.

The response of well water level to other aquifer pressure variations can be predicted as a function of frequency if the tidal phases and the ratio of the amplitudes of these two constituents can be fit to curves calculated from Eqs. (14) through (18) to estimate S and T. In practice, S cannot be estimated accurately from tidal response, as determined by Ritzi *et al.* (1991), who give an inversion algorithm for estimation of both these quantities.

4.2. Oscillations ("Hydroseismograms")

Coseismic water level oscillations in wells can be as large as several meters at teleseismic distances. These oscillations were first observed as vertical lines on analog hydrographs with low time resolution (the small upward fluctuation at the time of the earthquake in Fig. 1 probably represents such an oscillation). Blanchard and Byerly (1935) made higher speed recordings revealing that the oscillations resemble seismograms with dominant periods of 10 s or more. Rexin *et al.* (1962) present numerous examples of hydroseismograms. Figure 11a shows a high-speed recording of seismic oscillations in the Wali well near Beijing, China (Liu *et al.*, 1989).

Cooper *et al.* (1965) and Bredehoeft *et al.* (1965) gave the first analysis showing how the water column in a well of favorable dimensions in a very permeable formation could resonate at periods comparable to those of seismic Rayleigh waves. Liu *et al.* (1989) refined the analysis by Cooper *et al.* to obtain a more accurate estimate of the resonant period when the well is open to the aquifer over a long interval. Both analyses show that well water level can be amplified many times above the amplitude of pressure fluctuations in the aquifer.

The oscillatory well response depends on the same parameters as the wellbore storage response, and also on the height of the water column above the top of the aquifer. Consider a seismic wave with ground displacement, $u(t)$, having the form

$$u(t) = u_0 \exp(i\omega t), \tag{19}$$

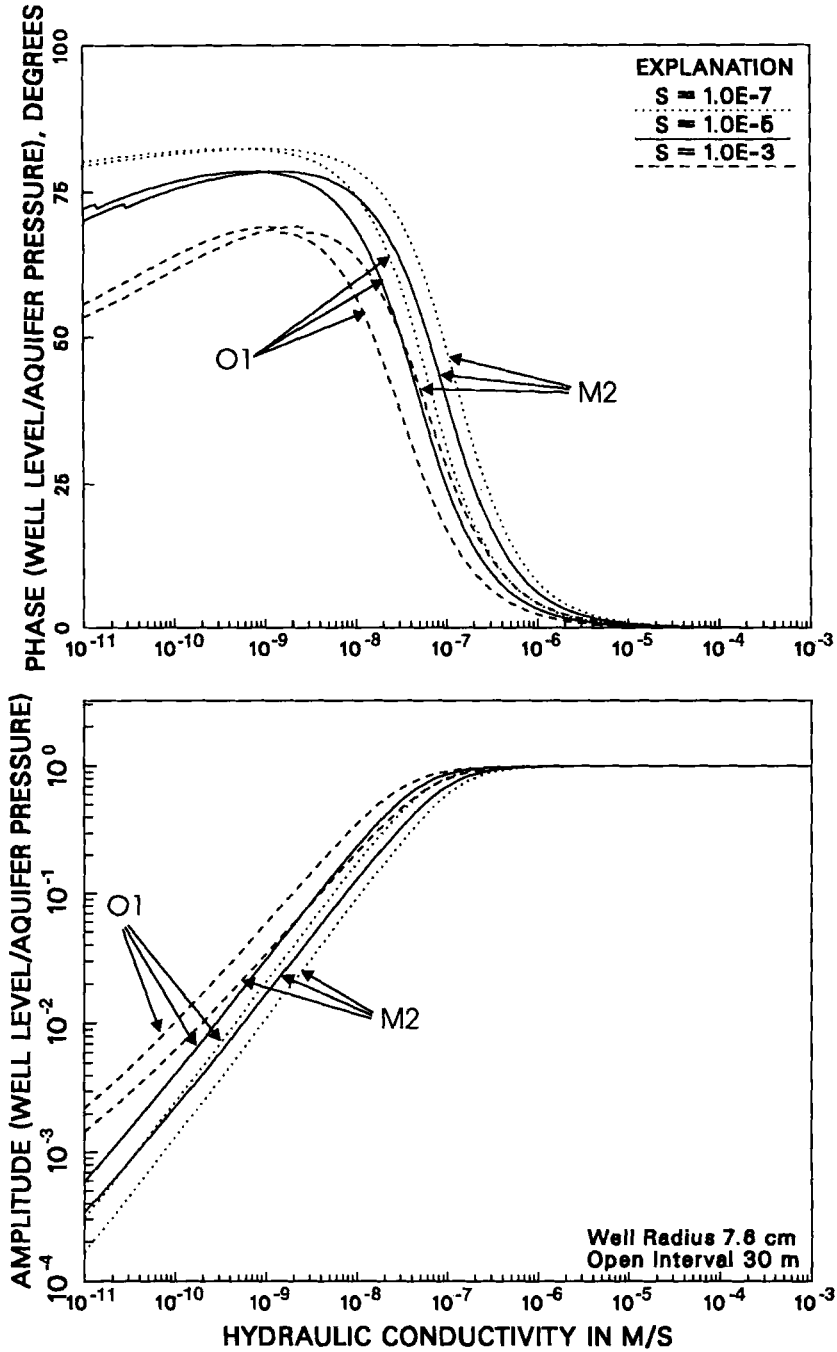

FIG. 10. Graph showing the effect of wellbore storage on the amplitudes and phases of diurnal and semidiurnal tide constituents for a well with a radius of 7.6 cm that is open over a depth interval of 30 m. Curves are plotted for three values of the storage coefficient, *S*. Positive phases denote a lag of well water level behind aquifer pore pressure.

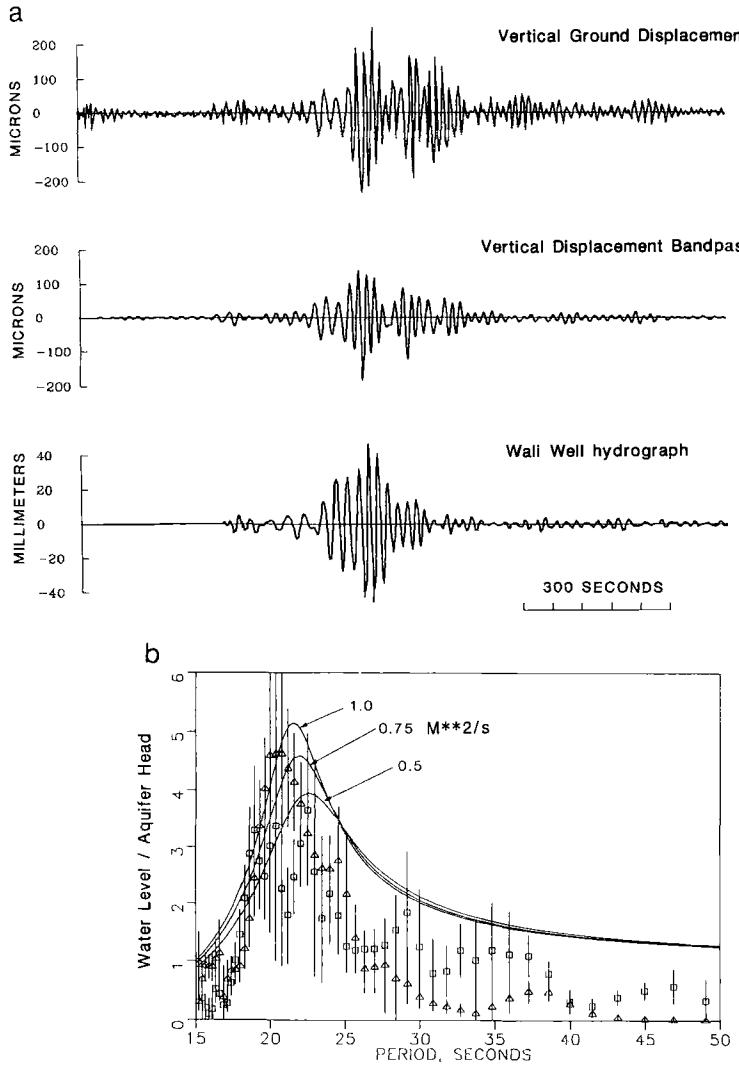

FIG. 11. (a) Seismograph from Baijiatan, China, and hydrograph from the Wali well near Beijing, China, for a magnitude 7.3 earthquake in the Kurile Islands (Liu *et al.*, 1989). (b) Graph showing estimates of the gain of the transfer function between well water level and aquifer pore pressure obtained by cross-spectral analysis of hydrographs and seismograms for two earthquakes, compared with the response calculated based on Eq. (22) (curves). Each curve is labeled with the assumed transmissivity. Other values used in Eq. (22) are $H = 92$ m, $d = 565$ m, $r_w = 0.117$ m, and $S = 5 \times 10^{-4}$. Triangles represent the response to a magnitude 7.3 earthquake in the Kurile Islands on March 24, 1984. Squares represent the response to a magnitude 7.1 earthquake in the West Irian region on November 17, 1985 (Liu *et al.*, 1989).

where u_0 is complex. The passage of the seismic wave causes a pressure head fluctuation, $h_0 \exp(i\omega t)$, in the aquifer, which in turn produces a water level fluctuation, $w_0 \exp(i\omega t)$, in the well. The ratio w_0/h_0 is the amplification of water level in the well relative to pressure head in the aquifer. For a well of radius r_w that fully penetrates an aquifer of thickness d and transmissivity T, Cooper *et al.* (1965) determined that

$$|w_0/h_0| = \left\{\left[1 - \frac{\omega r_w^2}{2T} kei(\alpha_w) - \frac{\omega^2 H_e}{g}\right]^2 + \left[\frac{\omega r_w^2}{2T} ker(\alpha_w)\right]^2\right\}^{-1/2}, \quad (20)$$

in which $H_e = H_w + 3d/8$ is the effective height of the water column in the well, and H_w is the height of the water column above the upper limit of the aquifer. Cooper *et al.* (1965) display curves based on Eq. (20) and show that for sufficiently high transmissivity there is a well-defined peak amplification at a frequency given by

$$\omega_w = (g/H_e)^{1/2}. \quad (21)$$

Liu *et al.* (1989) modified Eq. (20) to incorporate a more exact analysis of the flow field set up in the wellbore, needed when the length of the screened interval of the well is large. Their expression is

$$\frac{w_0}{h_0} = \left\{-\frac{\omega^2}{g}\left[H_w + \frac{1}{\gamma}\frac{1 - \exp(-\gamma d)}{1 + \exp(-\gamma d)}\right] - i\omega U r_w^2 \frac{\gamma \exp(-\gamma d)}{1 - \exp(-2\gamma d)} + 1\right\}^{-1}, \quad (22)$$

where $U = (d/T)[ker(\alpha_w) + ikei(\alpha w)]$ and $\gamma = (2i\omega/r_w^2 gU)^{1/2}$.

The data available to test Eqs. (20) and (22) consist of water level records, $w(t)$, and seismograms, $a(t)$. The ratio of seismically induced water level oscillations, w_0, to an oscillation at the same frequency in the seismograph record, a_0, can be written as

$$\frac{w_0}{a_0} = \frac{w_0}{h_0}\frac{h_0}{\epsilon_0}\frac{\epsilon_0}{u_0}\frac{u_0}{a_0}, \quad (23)$$

where ϵ_0 is the complex amplitude of dilatation in the aquifer.

Observations (Eaton and Takasaki, 1959) as well as theory suggest that water wells respond primarily to seismic surface waves with periods of 10 s or more. Surface waves consist of Love waves with horizontal motion perpendicular to the plane of propagation, and Rayleigh waves with retrograde ellipsoidal motion in a vertical plane containing the direction of

propagation (e.g., Bullen, 1979). Because Love waves have no associated dilatation, only Rayleigh waves are expected to cause water level oscillations in wells. For Rayleigh waves, the ratio of dilatation to ground displacement is given by

$$\frac{\epsilon_0}{u_0} = C\omega/v_R, \tag{24}$$

in which C depends on Poisson's ratio ν, v_R is the Rayleigh wave phase velocity, and u_0 is the vertical component of displacement upward taken positive (Ewing *et al.*, 1957; Bredehoeft *et al.*, 1965). As ν varies from 0.1 to 0.45, C takes on values from 0.665 to 0.009. Appropriate values for v_R are the phase velocities for continental Rayleigh waves given by Oliver (1962).

The ratio h_0/ϵ_0 is the response of pressure head to volume strain in the aquifer [Eq. (10)], which can be obtained from tidal analysis. The ratio u_0/a_0 is by definition the inverse of the seismograph magnification curve. Figure 11b compares the well response estimated from hydrograph–seismograph pairs for two earthquakes with Eq. (22).

For a well with a given geometry, the transmissivity is the most important factor governing the oscillatory response. As transmissivity increases, the amplitude of the peak response increases, and the peak response takes place at a shorter period. If the transmissivity is too low, the well will not be capable of an oscillatory response.

The mechanism described in this section predicts that water levels should return to their pre-earthquake values as soon as the surface wave train has passed and thus fails to explain the residual water level changes sometimes observed to follow the oscillations (e.g., Fig. 1; Davis *et al.*, 1955).

5. Coupled Flow and Deformation

5.1. Governing Equations

When stresses and strains vary with time, pore pressure no longer obeys the diffusion Eq. (12). Instead, p and σ_{kk} obey the coupled equation

$$c\nabla^2\left[\sigma_{kk} + \frac{3}{B}p\right] = \frac{\partial}{\partial t}\left[\sigma_{kk} + \frac{3}{B}p\right]. \tag{25}$$

Equivalently, the fluid mass obeys a diffusion equation under general conditions:

$$c\nabla^2 m = \frac{\partial m}{\partial t}. \tag{26}$$

Rice and Cleary (1976) give an exact expression for the diffusivity appearing in (25) and (26). However, Green and Wang (1990) have shown that if S_s is defined with the assumption of no deformation in two orthogonal directions and no stress change in the third orthogonal direction, then S_s may be expressed in terms of the poroelastic coefficients and, in fact, Eq. (13) holds. In particular, specific storage and hydraulic conductivity measured under conditions where vertical stress is fixed and there is no horizontal strain can be used to calculate diffusivity using (13). Such conditions are probably approximately met within several hundred meters of the earth's surface.

Equation (25) is sufficient to determine p when the mean stress field σ_{kk} is specified, or vice versa. But if additional components of the stress tensor are needed, then additional coupled equations are required (Rice and Cleary, 1976). These are the equilibrium equations and the compatibility equations:

$$\partial\sigma_{ij}/\partial x_j = 0, \tag{27}$$

$$\nabla^2\left[(1+\nu)\sigma_{ij} - \nu\sigma_{kk}\delta_{ij}\right] + \partial^2\sigma_{kk}/\partial x_i\partial x_i + \frac{3(\nu_u - \nu)}{B(1+\nu_u)}\left[\nabla^2 p\delta_{ij} + \partial^2 p/\partial x_i\partial x_j\right] = 0. \tag{28}$$

From (28), a useful relationship can be obtained by contracting indices:

$$\nabla^2\left[\sigma_{kk} + \frac{6(\nu_u - \nu)}{B(1-\nu)(1+\nu_u)}p\right] = 0. \tag{29}$$

5.2. Pore Pressure Changes Due to Strain or Fluid Influx

The porous elastic constitutive relations (4a and b) can be rearranged to express pore pressure change, p, in any porous elastic medium as

$$p = BK_u\left[-\epsilon_{kk} + \frac{1}{1 - K/K_s}\frac{m - m_0}{\rho_0}\right]. \tag{30}$$

Equation (30) is more general than Eq. (5b) because it has not been assumed that there is no change in fluid mass per unit volume. That is, Eq. (30) holds under any conditions ranging from drained to undrained. Equation (30) shows that pore pressure can rise due to contractional strain and/or from increasing the amount of fluid per unit volume.

Setting the right side of Eq. (30) to zero shows that flow out of a compressed porous elastic medium can relieve the pore pressure increase caused by strain if the volume of fluid outflow per unit volume is on the order of the volumetric strain, since $(1 - K/K_s)^{-1}$ is between one and five for most rocks. For example, fluid outflow of 10^{-6} m^3 per cubic meter of porous material can relieve 0.01 MPa of pore pressure, equivalent to a head drop of 1 m of water. In an aquifer 100 m thick with 10% porosity, this outflow will cause a water table rise of only 1 mm. In a poorly confined aquifer, fluid flowing from a compressed volume at depth moves upward toward the water table, but since a minute fluid outflow can relieve strain-induced pressure, no change in the water table is necessarily detected.

5.3. Water Table Aquifers and Confined Aquifers

A *confined aquifer* is usually defined as an aquifer sandwiched between two low-permeability units (aquitards). To add water to such an aquifer, pore pressure must rise as fluid is compressed. Here the term *confined* will be used more generally to describe any conditions under which the addition of water is accommodated by an increase in pore pressure and/or aquifer stress and strain. In contrast, a *water table aquifer* is one where added fluid is accommodated by a rise in the water table, which forms the aquifer's upper boundary.

This distinction is important in a study by Carrigan *et al.* (1991) of the possibility that very large water table excursions might be induced by earthquakes near the proposed nuclear waste repository at Yucca Mountain, Nevada. Carrigan *et al.* (1991) estimated the response of the water table to hypothetical slip along a normal fault equivalent to a magnitude 6.8 earthquake by simulating the groundwater flow field set up by the coseismic strain distribution. The events they considered that had uniform slip over the fault surface produced average static coseismic stress changes of 30 bars in the vicinity of the earthquake rupture, which, for a Skempton's coefficient of 1, would cause an undrained head increase in confined aquifers of about 300 m. Water table changes will be much smaller, however, because fluid can move into partially empty pore space above the water table. For the magnitude 6.8 earthquake, they found that the maximum water table rise was about 6 m.

6. Dissipation of Undrained Pressure by Flow to the Water Table

In studying a formation's response to subsurface strain it is important to recognize that every aquifer responds in a confined manner to disturbances with short enough timescales, but responds as a water table aquifer to sufficiently long-period disturbances, as illustrated in Fig. 12. This section describes how water table drainage affects the time-varying aquifer response to strain imposed by earth tides, barometric pressure, or earthquakes.

6.1. Water Table Drainage as a Function of Frequency

Consider an observation well open to the formation at depth z in an aquifer where z_w is the depth of the water table. The one-dimensional version of the differential equation (25) can be solved to give the response of aquifer pressure to a periodic strain variation (Bower and Heaton, 1978; Rojstaczer, 1988a). Suppose pore pressure and volumetric strain are harmonic functions of time, so that they can be expressed as $p_0(z)\exp(i\omega t)$ and $\epsilon_0 \exp(i\omega t)$, respectively. Boundary conditions are that $p_0(z_w) = 0$ and $p_0(\infty) = -BK_u\epsilon_0 \exp(i\omega t)$ (the undrained response). Substituting

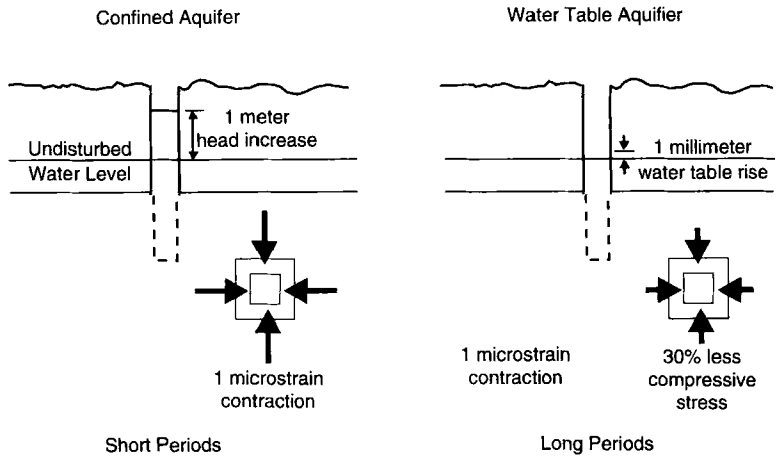

FIG. 12. Diagram illustrating the difference in behavior of confined versus water table aquifers.

these functional forms into (25) and expressing σ_{kk} in terms of p and ϵ_{kk}, by means of Eq. (4a), gives the ordinary differential equation

$$p_0''(z) = \frac{i\omega}{c}[p_0(z) + BK_u\epsilon_0]$$

to which the solution for the given boundary conditions is

$$\frac{p_0(z)}{\epsilon_0} = -BK_u\left[1 - \exp\left(-\left[i\omega(z - z_w)^2/c\right]^{1/2}\right)\right]. \tag{31}$$

It follows that for a strain signal with dominant frequency ω, the dimensionless quantity $\omega(z - z_\omega)^2/c$ is a useful measure of confinement. When $\omega(z - z_\omega)^2/c < 0.2$, the pressure disturbance induced by a strain episode will be less than $1/e$ of its value in a perfectly confined aquifer. Figure 13 illustrates the periods for which the amplitude of Eq. (31) is less than $1/e$ as a function of depth below the water table and hydraulic diffusivity.

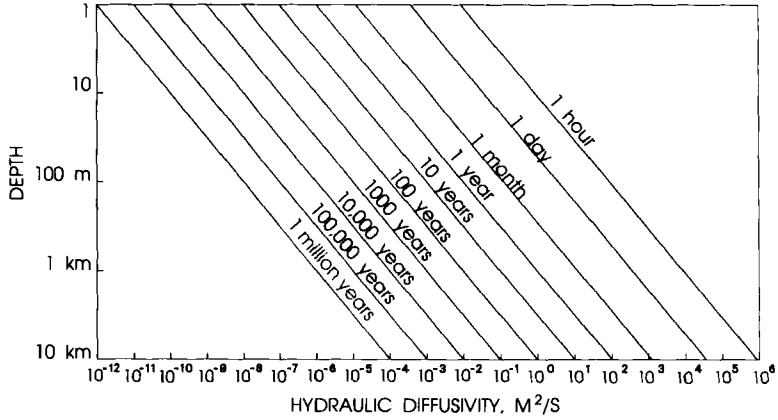

FIG. 13. Graph illustrating the relationship between depth below the water table, hydraulic diffusivity, and time scale of pore pressure dissipation to the water table. Each curve is given by $\omega(z - z_w)^2/c = 0.2$, for the indicated frequency, ω. If piezometer depth and aquifer diffusivity fall above the curve corresponding to a particular period, then flow to the water table will cause head disturbances due to strain having dominant frequency ω to be diminished by a factor of approximately $1/e$ with respect to the undrained value. Alternatively, the graph can be viewed as giving the elapsed time, t, after the imposition of a strain step such that the response has fallen to one-tenth of the undrained value, where t is approximately $11z^2/c$.

6.2. Hydraulic Diffusivity

The timescale of fluid flow in transient poroelastic problems is governed by the hydraulic diffusivity. As mentioned previously, Green and Wang (1990) have shown that hydraulic conductivities and storativities measured in most hydrogeologic tests can be used to obtain the diffusivity. Figure 14

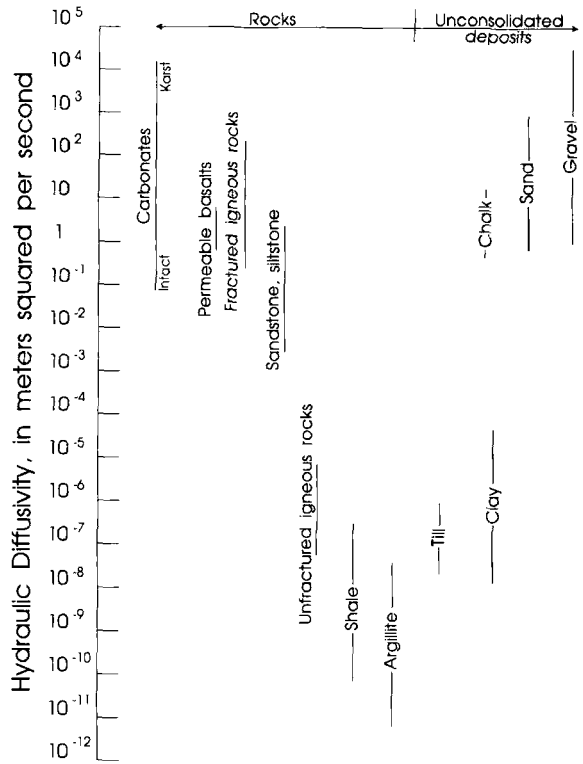

FIG. 14. Diagram illustrating observed ranges of hydraulic diffusivity as determined from field and laboratory studies. The ranges should not be considered limiting, because the number of measurements is small. Most values are from observations at several hundred meters or shallower depths. No attempt has been made to distinguish vertical and horizontal diffusivities. Data are from the following sources. Carbonates: Maslia and Prowell, 1990; Rasheeduddin *et al.*, 1989; Rojstaczer, 1987; Wei *et al.*, 1990. Sandstones and siltstones: Barrash and Ralston, 1991; Boehmer and Boonstra, 1987; Evans *et al.*, 1991b; Subyani and Sen, 1989. Basalts: Versey and Singh, 1982. Fractured igneous rocks: Andersson *et al.*, 1991; Boonstra and Boehmer, 1986; Rushton and Weller, 1985. Unfractured igneous rocks: Neuzil, 1986; Pickens *et al.*, 1987. Shale, argillite: Neuzil, 1986. Till: Keller *et al.*, 1989. Clay: Morin and Olsen, 1987; Neuzil, 1986. Chalk: Headworth *et al.*, 1982. Sand, gravel: Arad, 1983; Nativ and Gutierrez, 1989.

summarizes values of hydraulic diffusivity estimated from published values of hydraulic conductivity and storativity. These values range over 16 orders of magnitude, a range comparable to that of hydraulic conductivity or permeability.

In studies of seismicity induced by fluid injection, hydraulic diffusivity has been estimated as L^2/t, where L is the distance from the injection well to the earthquake activity, and t is the time elapsed between the beginning of injection and the onset of seismicity at distance L. For example, Fletcher and Sykes (1977) estimated diffusivities of 0.5 to 30 m^2/s for an area near the Clarendon–Linden fault in western New York state, comparable to values in the general range of 1 to 10 m^2/s at several other sites of induced seismicity. Based on cases of seismicity induced by fluid injection, Li (1984/85) has estimated diffusivities in the range of 0.1 to 1.0 m^2/s. These values are typical of sites in fractured crystalline rocks. The same technique can be applied to the estimation of diffusivity based on reservoir-induced seismicity, but because the weight of the reservoir imposes a stress change, pore pressure increases due to undrained compression would be expected to take place simultaneously with reservoir filling, so that L^2/t is a lower bound for the diffusivity (Roeloffs, 1988a). Talwani and Acree (1984/85) found that the areas of seismic activity for several reservoirs grew at rates suggesting diffusivities near 5 m^2/s, neglecting the pore pressure increase caused by compression. This upper bound value is consistent with the locations of many of these reservoirs on fractured crystalline rocks.

Most of the diffusivities shown in Fig. 14 are based on measurements at depths shallower than 1 km, and therefore are relevant to the behavior of water wells as strainmeters, but not necessarily to deeper processes. Fischer and Paterson (1992) have measured permeability and storativity for a marble, a sandstone, and a limestone at temperatures as high as 873 K. In tests at different effective pressures (confining pressure minus pore pressure), they observed that both permeability and storage capacity increased strongly as the effective pressure approached zero. They also found that the specific storage often decreases to a minimum and then increases as pore pressure is raised, which they attribute to competition between the tendency of the decreasing compressibility of the pore fluid to decrease storage, versus the tendency of increased porosity to increase storage.

The hydraulic conductivity (or permeability) is the property that governs steady-state flow. It is in general more easily determined than the storativity, but the majority of published values are for the high-permeability materials that constitute aquifers or hydrocarbon reservoirs. Values for

low-permeability environments are given by Brace (1980), Neuzil (1986), and Clauser (1992).

Where pore pressure in excess of hydrostatic persists for geologically long time periods, extremely low vertical hydraulic diffusivities or permeabilities are one possible explanation. Alternatively, Byerlee (1990) pointed out new laboratory evidence that at extremely low hydraulic gradients, Darcy's law no longer holds; instead, there is a "threshold gradient" below which flow ceases. This gradient has been measured to be as great as 0.5 MPa/m for clay with a void ratio of 0.75. If such a threshold gradient exists, then it would remove the need for extremely low diffusivities. Rice (1992) suggests alternatively that a steady supply of metamorphic fluids from greater depths might enable pore pressure to remain high in the core of a fault zone.

6.3. Effect on Well Tides of Flow to the Water Table

Equation (31) already shows how amplitude and phase vary due to flow to the water table to relieve strain. Evaluating this equation as a function of frequency shows that the aquifer pressure response decreases with increasing period and that the water level response leads the compressive strain signal. Figure 15 is a graph showing how these phase leads and amplitudes depend on $(z - z_w)^2/c$ at diurnal and semidiurnal frequencies. When flow to the water table is significant at tidal periods, M2 and O1 in the water level data will lead the corresponding constituents in the strain data. For almost all values of $(z - z_w)^2/c$, the phase lead will be larger for O1 than for M2 and the ratio of the water level tidal amplitude to the strain tidal amplitude will be smaller for O1 than for M2. Of course, if the vertical diffusivity is high enough, or if the well is shallow enough, then the effect of flow to the water table may be great enough so that no tides are recorded at all. In Fig. 3b, the tidal signal in the poorly confined Flinge Flat well is markedly smaller than at the other three sites, which are better confined.

6.4. Effect on Barometric Response of Flow to the Water Table

Barometric pressure disturbances associated with storms have periods of several days. In an imperfectly confined aquifer, drainage to the water table can reduce the aquifer pore pressure response to these longer period constituents of barometric pressure. The barometric pressure response then becomes a function of frequency, which is influenced by the vertical hydraulic diffusivity and in some cases by the diffusivity with respect to air

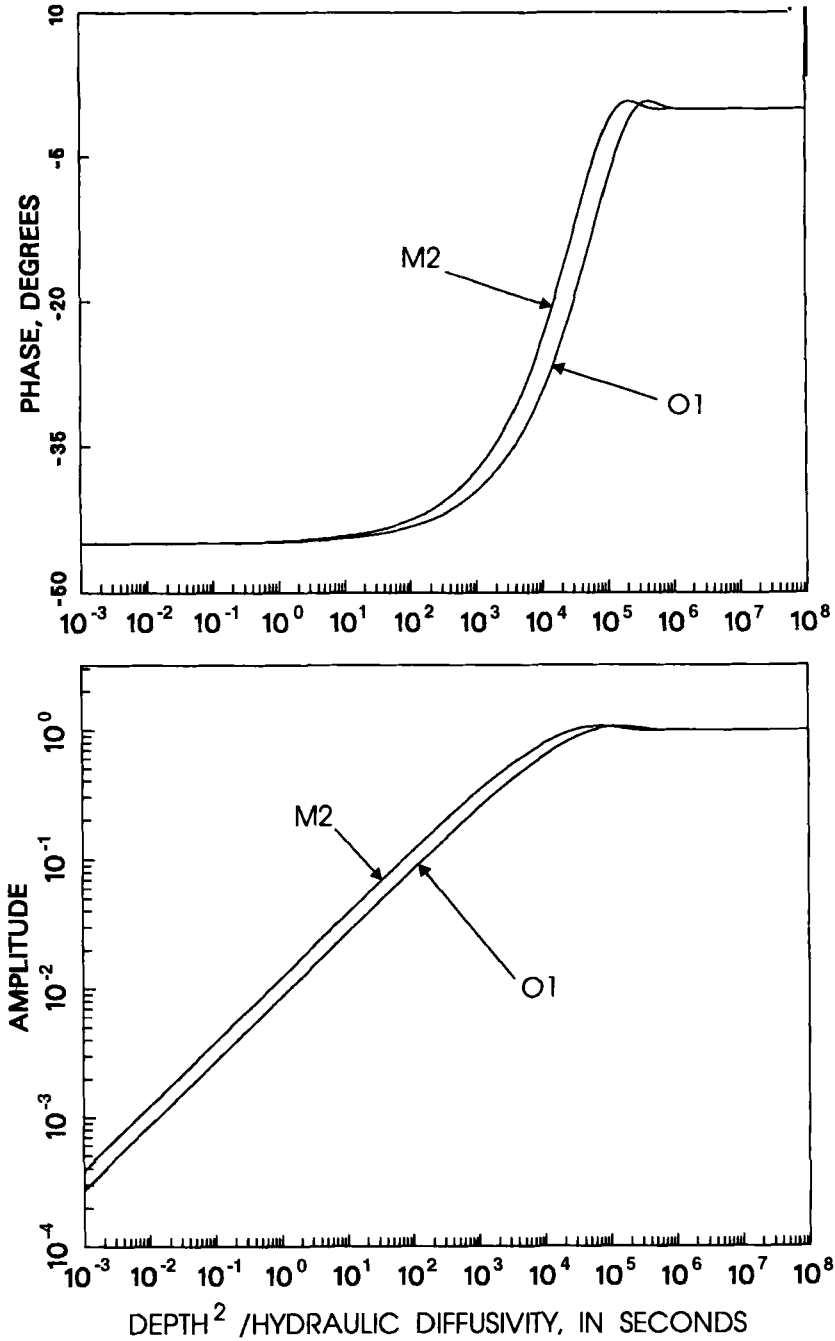

FIG. 15. Graph showing the effect of water table drainage on the amplitudes and phases of diurnal and semidiurnal tide constituents. Negative phases denote a lead of well water level with respect to aquifer pore pressure.

(the pneumatic diffusivity) of the unsaturated zone above the water table. Where long enough digital records of water level and barometric pressure are available, cross-spectral analysis of these data can yield the frequency-dependent transfer function between water level and barometric pressure (e.g., Bendat and Piersol, 1986). The vertical hydraulic and pneumatic diffusivities can be inferred from these transfer functions, and the vertical hydraulic diffusivity can then be used to estimate the well's response to strain as a function of frequency.

Bower and Heaton (1973), Weeks (1979), and Rojstaczer (1988b) have given equivalent expressions for the frequency-dependent barometric response of an imperfectly confined aquifer. Evans *et al.* (1991b) also presented an analysis of the frequency dependence of the barometric response, which extends the previous work by allowing for air wave attenuation at the capillary fringe above the water table and a low permeability "skin" where the wellbore is open to the formation. A summary is given next of the barometric response equivalent to the development by Rojstaczer (1988b) and Rojstaczer and Riley (1990), except that barometric pressure is treated as a source of volumetric strain, rather than areal strain. Further details of the derivation can be found in Quilty and Roeloffs (1991).

As in deriving the static confined barometric efficiency, the formation is taken to be laterally homogeneous and the barometric pressure is assumed uniform over an area that is large compared with the area of the aquifer affected by the well. Then, using Eqs. (5b) and (8), the volumetric strain induced in the aquifer is

$$\Delta\epsilon_{kk} = \frac{-(1-2\nu_u)}{2G(1-\nu_u)}\Delta b, \tag{32}$$

where $\Delta\epsilon_{kk}$ is independent of the depth in the aquifer since the barometric disturbance is assumed to be of infinite spatial extent. Consider periodically varying barometric pressure and pore pressure fields:

$$b = \tilde{b}e^{i\omega t}, \tag{33a}$$

$$p(z,t) = \tilde{p}(z)e^{i\omega t}. \tag{33b}$$

Since there is no lateral variation, substituting (32) and (33a and b) into (25) yields an ordinary differential equation for $\tilde{p}(z)$:

$$c\frac{d^2}{dz^2}\tilde{p}(z) - i\omega\tilde{p}(z) = -i\omega\frac{B(1+\nu_u)}{3(1-\nu_u)}\tilde{b}. \tag{34}$$

The general solution is of the form

$$\tilde{p}(z) = A_1 + A_2 \exp\left[-(i\omega/c)^{1/2}(z - z_w)\right], \tag{35}$$

where z_w is the depth from the earth's surface to the water table and A_1 and A_2 are constants determined from the following two boundary conditions. First, pore pressure and barometric pressure are equal at the water table:

$$\tilde{p}(z_w) = \tilde{b}. \tag{36}$$

Equation (36) implicitly assumes that barometric pressure at the water table is equal to barometric pressure at the earth's surface, that is, the pneumatic diffusivity of the unsaturated zone above the water table is high. Second, at infinite depth the pore pressure is the same as the static confined (undrained) pore pressure response given by Eq. (8):

$$\tilde{p}(\infty) = \frac{B(1 + \nu_u)}{3(1 - \nu_u)}\tilde{b}.$$

When A_1 and A_2 are determined, the pore pressure as a function of frequency and depth is

$$\frac{\tilde{p}(z)}{\tilde{b}} = \frac{B(1 + \nu_u)}{3(1 - \nu_u)} + \left[1 - \frac{B(1 + \nu_u)}{3(1 - \nu_u)}\right] \exp\left[-(i\omega/c)^{1/2}(z - z_w)\right]. \tag{37}$$

As in deriving Eq. (9), the water level change in a well, w_0, is proportional to the difference between the barometric pressure change at the water surface in the well and the pore pressure change where the borehole is open to the aquifer. The barometric efficiency can then be expressed as a function of frequency and depth as

$$E_B(z, \omega) \equiv \frac{\rho g \tilde{w}_0}{\tilde{b}} = -(1 - \alpha)\left[1 - \exp\left[-(i\omega/c)^{1/2}(z - z_w)\right]\right], \tag{38}$$

where α is defined in Eq. (8).

For finite pneumatic diffusivity, c_a, the air pressure above the water table becomes depth dependent. We assume the air pressure in the unsaturated zone, p_a, obeys the homogeneous diffusion equation

$$c_a \frac{\partial^2 p_a(z,t)}{\partial z^2} = \frac{\partial p_a(z,t)}{\partial t}. \tag{39}$$

Pressure p_a can also be expressed in the form

$$p_a(z,t) = \tilde{p}_a(z)e^{i\omega t}. \tag{40}$$

The solution to Eq. (39) is of the form

$$\tilde{p}_a(z) = D_1 \exp\left[(i\omega/c_a)^{1/2}(z - z_w)\right] + D_2 \exp\left[-(i\omega/c_a)^{1/2}(z - z_w)\right], \tag{41}$$

where D_1 and D_2 are determined from the boundary conditions. At the earth's surface the air pressure is equal to the barometric pressure:

$$\tilde{p}_a(0) = \tilde{b}. \tag{42}$$

The second boundary condition is that the water table is a no-flow boundary for air flow:

$$\left.\frac{d\tilde{p}_a}{dz}\right|_{z=z_w} = 0. \tag{43}$$

From these boundary conditions the particular solution to Eq. (39) is

$$\frac{\tilde{p}_a(z)}{\tilde{b}} = \frac{\exp\left[(i\omega/c_a)^{1/2}(z - z_w)\right] + \exp\left[-(i\omega/c_a)^{1/2}(z - z_w)\right]}{\exp\left[(i\omega/c_a)^{1/2} z_w\right] + \exp\left[-(i\omega/c_a)^{1/2} z_w\right]}. \tag{44}$$

At the water table (44) becomes

$$\frac{\tilde{p}_a(z_w)}{\tilde{b}} = \frac{2}{\exp\left[(i\omega/c_a)^{1/2} z_w\right] + \exp\left[-(i\omega/c_a)^{1/2} z_w\right]}. \tag{45}$$

A barometric efficiency combining the effects of finite pneumatic diffusivity and flow to the water table can be derived by replacing the boundary condition (36) by

$$\tilde{p}(z_w) = \tilde{p}_a(z_w). \tag{46}$$

Equation (38) then generalizes to

$$\frac{\tilde{p}(z)}{\tilde{b}} = \frac{B(1 + \nu_u)}{3(1 - \nu_u)} + \left[\frac{\tilde{p}_a(z_w)}{\tilde{b}} - \frac{B(1 + \nu_u)}{3(1 - \nu_u)}\right] \exp\left[-(i\omega/c)^{1/2}(z - z_w)\right]. \tag{47}$$

The expression for barometric efficiency corresponding to (47) is

$$E_B(z, \omega) = -1 + \alpha + \left[\frac{\tilde{p}_a(z_w)}{\tilde{b}} - \alpha\right] \exp\left[-(i\omega/c)^{1/2}(z - z_w)\right], \tag{48}$$

where $\tilde{p}_a(z_w)/\tilde{b}$ is Eq. (45).

Rojstaczer (1988b) shows type curves generated by plotting barometric efficiency as a function of two dimensionless frequencies: $Q = \omega(z - z_w)^2/2c$ and $R = \omega z_w^2/2c_a$. The ratio R/Q is a measure of the time taken for the diffused air molecules to pressurize the water table versus the time taken for water table flow to the unsaturated zone to relax the initial undrained pore pressure response of the aquifer. Evans *et al.* (1991b) illustrate the various shapes the barometric response curve takes when the effects of water table leakage, finite pneumatic diffusivity, and wellbore storage are combined.

If pneumatic diffusivity becomes negligible, Eq. (48) reduces to

$$E_B(z, \omega) = -1 + \alpha\left\{1 - \exp\left[-(i\omega/c)^{1/2}(z - z_w)\right]\right\}. \tag{49}$$

All three relationships for barometric efficiency—Eq. (38), (48), and (49)—approach $-1 + \alpha$ as z or ω become large.

A well's response to barometric pressure, when it can be determined as a function of frequency, yields an estimate of c (e.g., Rojstaczer, 1988a,b); a barometric response that has decreasing gain as periods lengthen is diagnostic of a partially confined aquifer. A barometric response that does not fall off at long periods proves that the aquifer behaves in a confined manner over time periods as long as the longest period constituents in the barometric pressure record, which are of the order of 10 to 30 days. Evans *et al.* (1991a) were able to use well-level fluctuations induced by the rise and fall of Lake Nasser to show that a 400-m-deep well in the Nubian formation is well confined at periods as long as several years.

6.5. Water Table Drainage as a Function of Time

The response as a function of time to a unit strain step can be obtained from (31) by replacing $i\omega$ with the complex variable s, multiplying by $1/s$, and inverting the resulting Laplace transform to obtain

$$p(z, t) = -BK_u\epsilon_0 \operatorname{erf}\left\{\left[(z - z_w)^2/4ct\right]^{1/2}\right\}, \tag{50}$$

where erf denotes the error function (Abramowitz and Stegun, 1972). Figure 16 is a graph of Eq. (50) as a function of time. Bower and Heaton (1978) developed an expression similar to Eq. (50) and showed that it could match the observed response of the Ottawa well to the Alaska earthquake (Fig. 1), suggesting that the change was caused by strain.

Equation (50) shows that the time required for a strain-induced pressure increase to dissipate, resulting in a minute, probably undetectable, water table rise, is inversely proportional to the (vertical) hydraulic diffusivity of

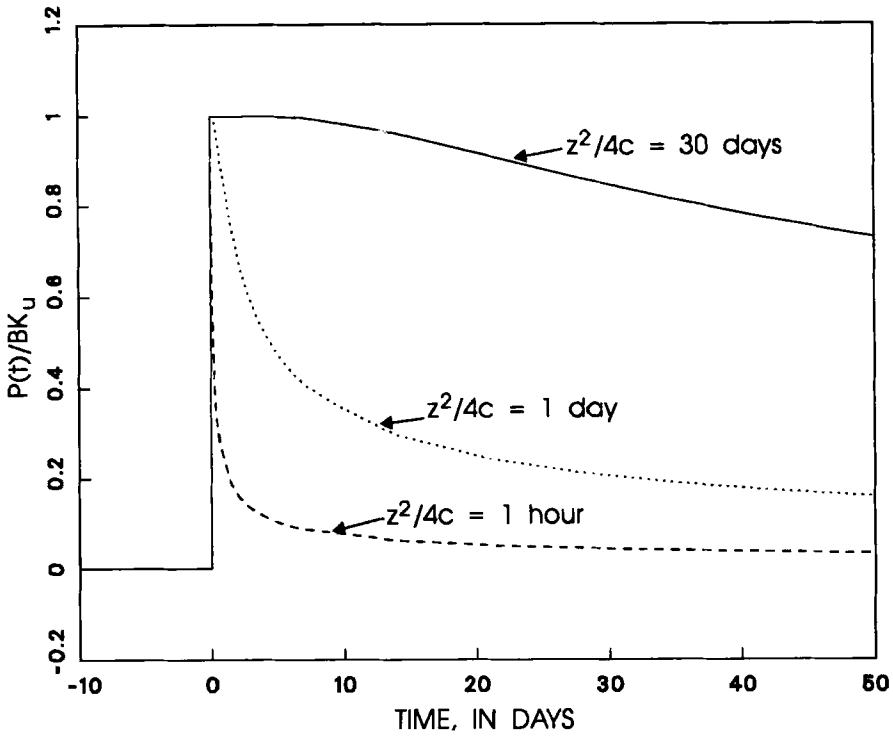

FIG. 16. Graph showing the response of a partially confined aquifer to volumetric strain with a step-function time history, for several values of $z^2/4c$.

the aquifer and directly proportional to $(z - z_w)^2$. More specifically, the pore pressure response will have decayed to one-tenth of the undrained value when elapsed time, t, is approximately $11(z - z_w)^2/c$. Figure 13 illustrates the relationship between depth, diffusivity, and the timescale of pore pressure dissipation by flow to the water table.

Equation (50) shows that pressure changes due to strain cannot last indefinitely in an imperfectly confined aquifer, and thus in turn implies that long-term pressure changes in such aquifers are caused by other mechanisms. For example, if enough fluid enters the aquifer to raise the water table 1 m, then the pressure will rise 0.01 MPa due to the weight of the added water.

Equations (30) and (50) provide ways to estimate the diffusivity. Water level tides that lead the *in situ* volumetric strain tide are characteristic of partially confined aquifers; c can be estimated by comparing observed phase leads with those predicted by Eq. (31), and c can be chosen so that

the observed response to a strain step matches Eq. (50) or the corresponding response obtained numerically for a finite-length open interval (e.g., Roeloffs *et al.*, 1989).

7. Flow Accompanying Fault Movement

7.1. Water Level Changes Associated with Fault Creep

Fault creep is slip of one side of a fault plane relative to the other that takes place too slowly to generate seismic waves. Along the San Andreas fault in north central California, creep often takes place in "events" entailing up to several millimeters of movement over a period of hours to days. Some creep events are recorded at a single creepmeter, but other events appear to propagate along the fault. Creep events have not been recorded anywhere except in California (on the San Andreas, Calaveras, Hayward, and Garlock faults) but may occur in other tectonically active areas.

Johnson *et al.* (1973) presented the first model analysis of water level changes due to fault creep on the San Andreas fault. Groundwater level fluctuations in a well near the Garlock fault in California were fit to theoretical curves developed for several idealized models of creep events (Lippincott *et al.*, 1985; Rudnicki and Hsu, 1988), and Ben-Zion *et al.* (1990) report water level fluctuations in a well in the Mojave Desert that resemble creep-induced water level changes, but in these two cases, no nearby creepmeter was available to demonstrate the occurrence of fault creep. Figure 17 shows creep, water level, and borehole strain records for a creep event on the San Andreas fault near Parkfield, California.

Like an earthquake, the slip that takes place in a creep event can be modeled as a dislocation. Cleary (1977) has given the three-dimensional solution for the stress, strain, and pore pressure fields created by a point dislocation in a poroelastic full space. Observed creep-related water level changes, however, have generally been modeled using two-dimensional solutions for instantaneously introduced and propagating dislocations. Rice and Cleary (1976) gave the plane-strain solution for the pore pressure field produced by a shear dislocation instantaneously introduced into a poroelastic full space. With reference to the coordinate system shown in Fig. 18, this solution is

$$p(x, y, t) = \frac{\alpha G \Delta u}{\pi}(y/r^2)[1 - \exp(-r^2/4ct)]H(t), \qquad (51)$$

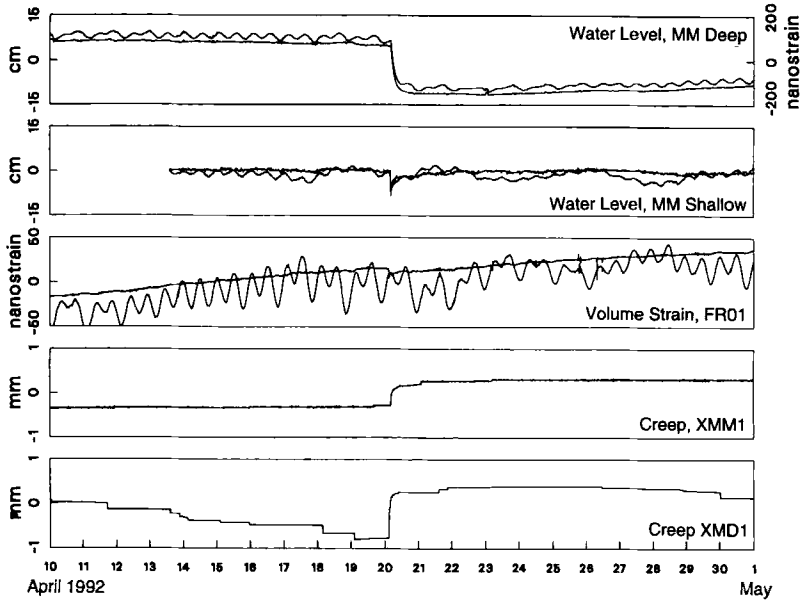

FIG. 17. Graph showing water level data from two levels of the Middle Mountain well near Parkfield, California, compared with records from a borehole strainmeter and two creepmeters. Water level and strain data are shown both before and after removal of tidal and barometric effects. The borehole strain record has been expressed in units of strain by equating the amplitude of its M2 constituent to that of the equilibrium volume strain tide. The strain scale for the deep well interval has been determined by equating the amplitude of M2 in the water level data with that of the borehole strain record.

where Δu is the relative slip imposed on the negative y-axis, and $H(t)$ is the unit step function. Equation (51) was developed under the assumption that the fault plane is permeable. The solution changes sign depending on the sense of the offset (right- or left-lateral) and is antisymmetric with respect to the fault plane.

The corresponding expression for a shear dislocation on an impermeable fault plane is (Rudnicki, 1986):

$$p(x,y,t) = \frac{\alpha G \Delta u}{\pi}(y/r^2)\Big\{\operatorname{erf}\big[y/(4ct)^{1/2}\big] + (2x/\pi^{1/2}r^2)\exp(-y^2/4ct)\operatorname{Daw}\big[x/(4ct)^{1/2}\big]\Big\}, \tag{52}$$

where $\operatorname{Daw}(\xi)$ is Dawson's integral, given by

$$\operatorname{Daw}(\xi) = e^{-\xi^2}\int_0^{\xi} e^{\eta^2}\, d\eta$$

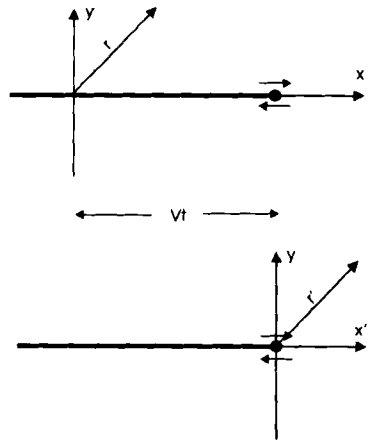

FIG. 18. Coordinate systems for dislocation models of water level changes due to fault creep. Slip extends from $x - Vt = 0$ along the negative x-axis and is in the sense shown.

(Abramowitz and Stegun, 1972). Rudnicki (1987) describes solutions corresponding to (51) and (52) for instantaneously introduced opening-mode dislocations on permeable and impermeable faults.

Since different solutions are needed for creep events on permeable as opposed to impermeable faults, it is natural to ask whether the form of a creep-related water level change can reveal whether the fault plane is permeable or not. Rudnicki *et al.* (1993) compared solutions for permeable and impermeable fault planes to creep-related water level changes recorded in the Middle Mountain well in Parkfield, California (e.g., Fig. 17). They found that the data could be fit equally well by either solution, although a higher diffusivity is required if the fault plane is assumed to be impermeable. Independent of the assumption about the fault plane permeability, the location on the fault of the tip of the slip zone could be estimated from the rate at which the pore pressure returned to normal following the creep event.

Some creep events appear to propagate along the fault and thus can be approximated as steadily moving dislocations. If V is the constant velocity of propagation, then it is useful to use the new coordinates $x' = x - Vt$ and $r' = [(x')^2 + y^2]^{1/2}$. The pore pressure field produced by such a propagating creep event on a permeable fault plane can be obtained from (51) by superposition to obtain

$$p(x', y) = \alpha G \Delta u / \pi \left(y/r'^2\right)[1 - (Vr'/2c)K_1(Vr'/2c)\exp(-Vx'/2c)], \tag{53}$$

where K_1 denotes the modified Bessel function of the second kind (e.g., Roeloffs and Rudnicki, 1984/85). The solution changes sign depending on the sense of the offset (right- or left-lateral) and is antisymmetric with respect to the fault plane. Rudnicki and Roeloffs (1990) give the corresponding solution for an impermeable fault plane.

Figure 19a illustrates the form that the pore pressure disturbance due to a propagating creep event might have. Total offset in the creep event is 1 mm, and the aquifer pressure disturbance is shown for two distances, y, from the fault plane. Five km from the fault plane, the solutions for the permeable and impermeable fault planes are indistinguishable. But for $y = 1$ km, the permeable fault plane solution has a pronounced sign change and a smaller peak than the impermeable fault plane solution. Figure 19b shows the water level response in a well that has non-negligible wellbore storage effects at periods near one day. For this case, the effect of wellbore storage reduces the amplitude by a factor of about two, and makes the sign change of the permeable fault plane solution less apparent. This figure illustrates why it could be difficult to use fault creep and water level data to distinguish whether the permeable or impermeable solution is more appropriate.

For events involving slip over a finite area of a fault plane, solutions can be constructed by integration (usually numerical) of the elemental dislocation solutions (e.g., Rudnicki and Hsu, 1988). Numerical methods are also necessary to model creep events in porous elastic half spaces. In practice, flow to the earth's surface would be expected to modify the pore pressure field accompanying a fault creep event. The creep-related water level change shown in Fig. 17 was recorded at two different depths in a well near Parkfield, California. Flow to the water table causes the pore pressure in the shallow interval to recover within hours, whereas pressure in the deeper interval remains low for days to weeks. The eventual return of water level in the deep interval to its pre-event value may be due to horizontal flow, to flow to the water table, or to a combination of the two effects (Roeloffs *et al.*, 1989).

Coupling of deformation with pore fluid diffusion provides one possible reason why fault creep events propagate stably without developing into seismic ruptures. A porous elastic medium has a greater effective stiffness in response to undrained deformation than drained deformation. As a crack propagates in such a medium, the energy required to advance increases with propagation velocity over the range of velocities that have been observed for propagating creep events (Rice and Simons, 1976). This effect, which tends to discourage acceleration of the crack front, takes place for both permeable and impermeable faults. Rudnicki and Koutsibelas (1991) showed, however, that for impermeable faults, changes

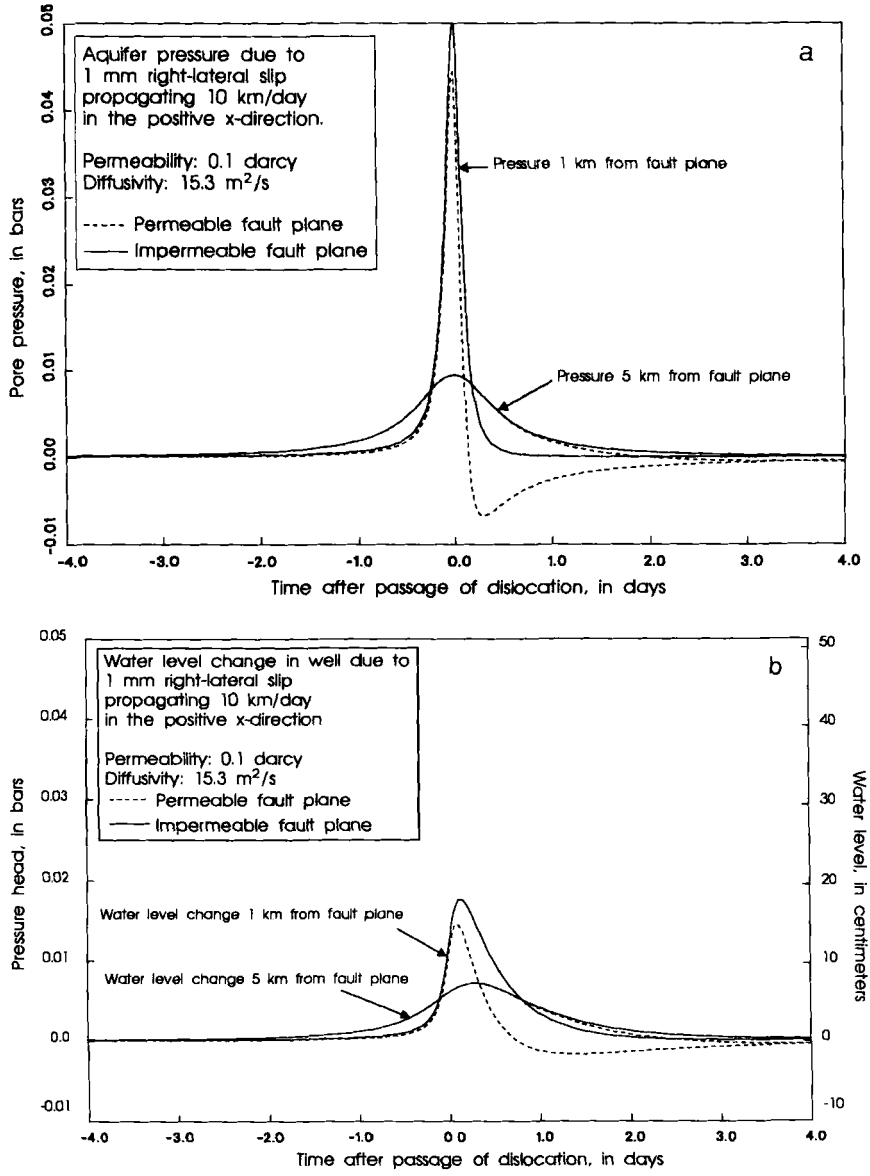

FIG. 19. (a) Graph showing hypothetical histories of aquifer pore pressure measured 1 and 5 km from a vertical strike-slip fault. (b) Well water level fluctuation expected in response to the pore pressure variations shown in part (a), for a well with significant wellbore storage.

of pore pressure on the fault plane must also be considered in evaluating whether pore fluid diffusion causes the resistance to propagation to increase or decrease with increasing speed. For a shear crack on an impermeable fault plane, pore pressure changes on the two sides of the plane are equal and opposite. Resistance to sliding will be decreased on the side of the fault plane where pore pressure increases, which may result in a net destabilization and contribute to the development of a seismic rupture.

7.2. Fluid Flow Following Earthquakes

As fluid flow takes place around a slip zone, the stress state on the slipping zone changes. A number of investigators have considered how this stress redistribution might affect aftershocks or the foreshock–mainshock relationship.

Nur and Booker (1972) and Booker (1974) evaluated the pore pressure, stress, and strain fields following uniform, instantaneous slip over a two-dimensional planar fault in a porous elastic medium. They showed that the equilibration of the pore pressure field caused by slip would be expected to reload the fault, but by an amount equal to at most half of the seismic stress drop. To explain how this reloading might cause aftershocks, Booker (1974) postulated that the postearthquake frictional resistance of the fault might be nonuniform, with some areas able to fail if reloaded by only a fraction of the initial stress drop.

Hudnut *et al.* (1989) explored the possibility that pore pressure changes governed the timing of the magnitude 6.6 Superstition Hills earthquake relative to the magnitude 6.2 Elmore Ranch earthquake 11.4 hr earlier. Because the two faults are orthogonal and intersecting, left-lateral slip on the Elmore Ranch fault had an "unclamping" effect on the Superstition Hills fault. Calculations suggest that immediately following the Elmore Ranch earthquake, this decrease in normal stress was counteracted by a decrease in pore pressure due to undrained extension, and the Coulomb stress assumed its most critical value at a location just south of the intersection of the two faults. For several sets of poroelastic material properties, the Coulomb stress increased by 20–25% of the earthquake stress drop as the pore pressure recovered in the hours following the Elmore Ranch earthquake. A diffusivity of 5 m^2/s causes the final value to be reached 11.4 hr after the Elmore Ranch event, when the Superstition Hills earthquake nucleated at that location.

Jaumé and Sykes (1992) and Stein *et al.* (1992) have considered the role of pore pressure changes due to undrained deformation in calculations of

the coseismic Coulomb stress changes on major faults due to the 1992 Landers earthquake sequence. Jaumé and Sykes hypothesize that a 60-km-long segment of the San Andreas fault will be brought closer to failure as pore pressure lowered by coseismic extension reequilibrates to its pre-earthquake value.

The studies described above have assumed that the fault plane is highly permeable relative to its surroundings. Rudnicki (1986) has shown that an impermeable fault plane would be expected to behave somewhat differently. In particular, on the permeable fault plane, shear stress induced by slip decays monotonically, whereas on the impermeable fault plane, the shear stress increases for a period of time before decreasing, and is always greater than if the fault plane were permeable. The analytic solution used in these studies also neglects vertical flow. But in the numerical modeling study by Carrigan *et al.* (1991) of flow following a hypothetical earthquake near Yucca Mountain, it was found that in the absence of anisotropy, flow is predominantly horizontal rather than vertical.

Although these models are physically appealing, the data to test them adequately do not yet exist. As described in the next section, many coseismic water level changes do not resemble the model outlined here or in Section 3.7.

7.3. Unexplained Observations

Among the more dramatic effects of earthquakes on hydrology are streamflow increases within a distance of one to two source dimensions of earthquakes having various focal mechanisms. The Borah Peak, Idaho, earthquake, which was a normal faulting event, increased discharges from carbonate springs and river base flows. These effects diminished exponentially over the next six months to their pre-earthquake levels. Muir-Wood and King (1993) describe several examples of enhanced stream discharge following earthquakes and suggest that the most significant response is found to accompany major normal fault earthquakes. The 1991 $M_s = 6.2$ Honeydew earthquake, in northern California, caused discharge in the Mattole river to more than double over the following 6 days, with a decay to pre-earthquake levels in about 6 weeks (McPherson and Dengler, 1992), showing that postearthquake discharge increases are possible for reverse-faulting events as well.

Permeability enhancement due to strong earthquake shaking is a mechanism that may occur irrespective of focal mechanism, as hypothesized by Rojstaczer and Wolf (1992) for the Loma Prieta event. Sibson (1990, 1992) suggested that fluid efflux following earthquakes could be due to the

collapse of pore space that opened in response to high levels of shear stress immediately preceding the earthquake (dilatancy). Alternatively, he suggested that fracturing caused by the earthquake could cause the fault itself to act as a high-permeability conduit for high-pressure fluids moving upward from depth, with sealing eventually causing the fault to become impermeable. The possibility that increased discharge originates at seismogenic depths is intriguing, but did not appear to be the case for the Loma Prieta event; geochemical studies after future earthquakes are needed to establish the source of such fluids.

Kawabe *et al.* (1988) describe a coseismic flow increase from an artesian well 226 km northeast of a magnitude 6.6 normal faulting earthquake on March 18, 1987, in southwest Japan. They evaluated the relation between flow rate and tidal strain, and on this basis found that the total increase in flow rate was 40 times too large to be accounted for by the residual strain field of the earthquake. This observation is far enough from the earthquake epicenter that fracturing associated with faulting is unlikely to be the cause.

Observations like the one by Kawabe *et al.* (1988) may be related to transient increases or decreases of static water level following distant earthquakes, like the one shown in Fig. 1. In many cases, these transient changes follow oscillations, which are potentially explained by the mechanism outlined in Sec 4.2, involving resonant motion of the water in the well casing. Responses to distant earthquakes along the margins of the Pacific, North American, and Cocos plates have also been observed in Devil's Hole, a natural pool in Death Valley, California (Galloway and Wilcoxon, 1993). Figure 20 shows water level rises in a well near Parkfield, California, in response to earthquakes in several parts of California. To date, there is no satisfactory explanation for coseismic hydrologic changes that persist beyond the duration of the earthquake's surface wave train.

8. Hydrologic Earthquake Precursors

An intriguing and important question is whether hydrologic phenomena precede earthquakes. Because earthquakes *produce* hydrologic changes at great distance, it has been suggested that hydrologic changes can forecast earthquakes at great distance. Many hydrologic changes preceding earthquakes have been reported, but in most cases, the documentation has not been sufficient to convince the scientific community that these phenomena should have been considered warnings of an impending seismic event.

One plausible mechanism for water level changes preceding earthquakes is preseismic volumetric strain. Because wells differ in their degrees of confinement, not all wells are equally likely to respond to volumetric

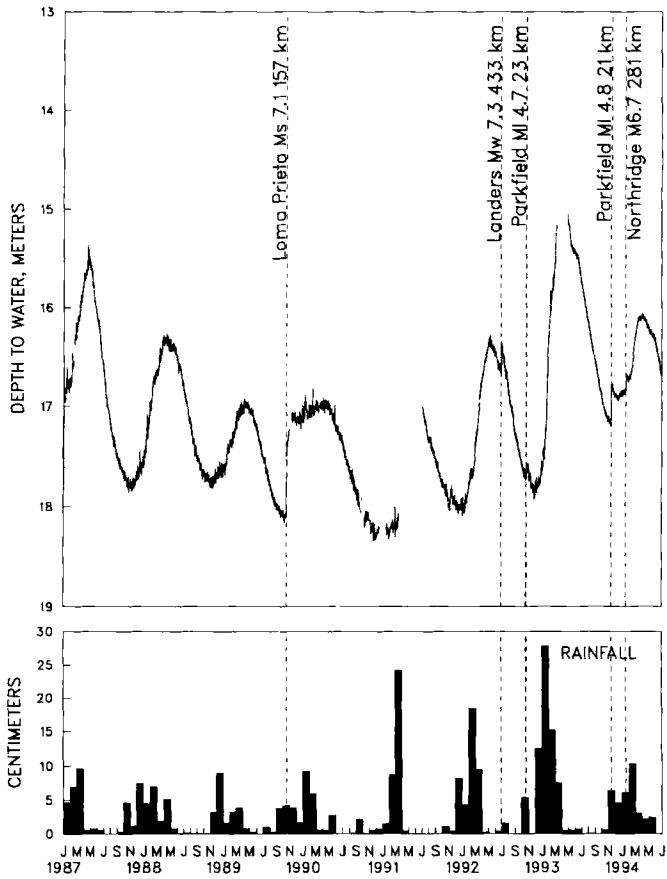

FIG. 20. Hydrograph from the Bourdieu Shallow well near Parkfield, California (BS in Fig. 3a). The well has experienced several rises in water level at the times of distant earthquakes.

strain, particularly if it takes place over a period of several days or more. For example, water level changes lasting three days preceded the 1985 Kettleman Hills, California, earthquake in two relatively well-confined aquifers (Figs. 3b and 8), but were not observed in two other wells being monitored. The Flinge Flat well, which did not display the anomaly, can be shown on the basis of its tidal and barometric responses to be so poorly confined that it could not have responded to a volumetric strain change taking place over three days. The Turkey Flat well is also poorly confined, but a response to the anomaly should have been detectable, although at only about half the amplitude of the response in the Gold Hill or Joaquin Canyon wells. Figures 21a, b, and c show the hypothetical response to a

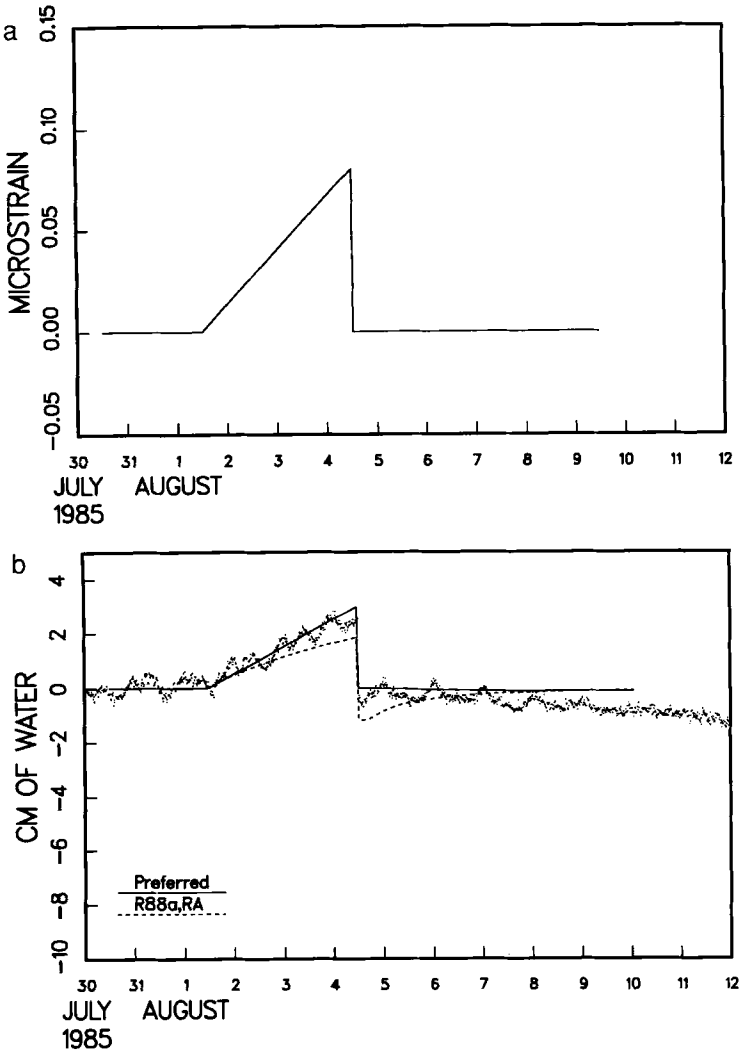

FIG. 21. (a) Hypothetical preseismic and coseismic strain history for the Parkfield area at the time of the Kettleman Hills earthquake. (b) Predicted response of water level in the Joaquin Canyon well to the strain history shown in part (a), compared with the observed water level. Tides and barometric pressure effects have been subtracted from the observed water level data, and the data have been referenced to their average value for the period July 29 through July 30. For Joaquin Canyon only, a linear function representing the hydrologic trend has also been subtracted from the data.

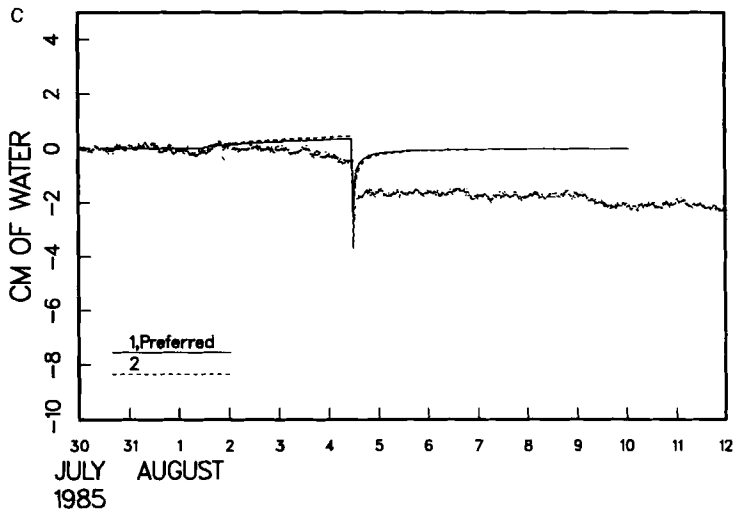

FIG. 21. (c) Predicted response and observed water level for Flinge Flat. (Roeloffs and Quilty, 1995).

volumetric strain signal that ramps up over three days in the Joaquin Canyon and Flinge Flat wells, respectively. The responses were obtained from the wells' tidal and barometric responses, as derived in Roeloffs and Quilty (1995).

The principle that imperfect confinement limits response at long periods can sometimes be applied to evaluate published reports of earthquake precursors. For example, declining water levels near the city of Tianjin beginning four and one-half years before the 1976 Tangshan, China, earthquake were observed in wells 63 to 100 m deep (Figs. 2a and b). If the declining water levels were due to extensional strain, then vertical hydraulic diffusivity must have been low enough to prevent leakage to the water table. In particular, the 4.5-yr time interval must be less than $11z^2/ct$, so that the diffusivity of the material overlying the aquifers would have to be less than 8×10^{-4} m^2/s. Figure 14 shows that such low diffusivities are plausible only for argillaceous materials or crystalline rocks without significant fracturing. Either layers of very low diffusivity material are present, or these changes cannot have been caused by strain.

Roeloffs (1988b) pointed out that if groundwater level changes preceding earthquakes are due to elastic strain in response to preseismic fault slip, they should be no larger than coseismic water level changes, which can in principle be estimated from a typical aquifer sensitivity to volumetric strain and a plot of volumetric strain for the earthquake. Very few

reported anomalies meet this criterion. On the other hand, it is now clear that water level changes produced by earthquakes are both larger and of longer duration than would be expected based on the principles outlined in Section 3.7. Many more reports meet the criterion of being smaller than the observed, rather than theoretical, coseismic response (excluding oscillations). On the other hand, the observation that well levels and stream discharges can respond strongly to distant earthquakes suggests that teleseismic events need to be eliminated as possible causes of anomalies before concluding that they are earthquake precursors.

Little work has been done to interpret quantitatively reports of discharge changes preceding earthquakes, such as the citizen's report before the Loma Prieta earthquake (Roeloffs, 1993). Kawabe *et al.* (1988) observed a small increase before a large coseismic increase in discharge from an artesian well in Japan. In neither of these cases are the data ideal, but the similarities between the observations increases their credibility and suggests that a common mechanism could be operating.

9. Summary

This paper has described the range of earthquake-related hydrologic phenomena, outlined the poroelastic techniques that exist for interpreting them, and pointed out where these techniques are inadequate. Most of the analysis techniques described here require digital data sets, and some, such as cross-spectral analysis to estimate long-term strain sensitivity, require data sets on the order of a year in duration. But where data are recorded in a suitable way, quantitative techniques are available to relate the data to crustal strain. The utility of a water well as a strainmeter is limited by the aquifer's degree of confinement, and may also be limited by severe wellbore storage effects.

Data collected and analyzed to date show that earthquakes have hydrologic aftereffects that are not explained adequately by poroelastic theory, and indeed do not seem to be elastic. Further work is needed to understand these phenomena and determine how they may be related to the generation of natural earthquakes or to the observability of earthquake precursors.

The question of the existence of hydrologic earthquake precursors has not yet been answered definitively, in large measure because reported precursors are still inadequately documented. However, there are similarities between reports of discharge increases preceding earthquakes, and high-resolution data collected at Parkfield, California, facilitated documentation of water level changes preceding the 1985 Kettleman Hills

earthquake. In evaluating reports of groundwater level changes before earthquakes, the aquifer's degree of confinement, response to strain, and history of coseismic changes can illuminate the mechanism of the water level change. Because potential observations of precursors could be scientifically valuable, they deserve scrutiny even when the quality of data is poor.

ACKNOWLEDGMENTS

Many of the topics described here evolved from original work or suggestions by John Bredehoeft, who also initiated the data collection effort in California that has made it possible to test and refine these techniques. Ruth Harris, John Rudnicki, Joseph Walder, and an anonymous reviewer provided comments that facilitated improvement of the manuscript.

REFERENCES

Abramowitz, M., and Stegun, I. A. (eds.). (1972). "Handbook of Mathematical Functions." Appl. Math. Ser. 55, National Bureau of Standards, Washington, DC.

Andersson, J.-E., Ekman, L., Nordqvist, R., and Winberg, A. (1991). Hydraulic testing and modeling of a low-angle fracture zone at Finnsjon, Sweden. *J. Hydrol.* **126,** 45–77.

Arad, A. (1983). A summary of the artesian coastal basin of Guyana. *J. Hydrol.* **63,** 299–313.

Barrash, W., and Ralston, D. R. (1991). Analytical modeling of a fracture zone in the Brule Formation as an aquifer receiving leakage from water-table and elastic aquitards, *J. Hydrol.*, **125,** 1–24.

Beaumont, C., and Berger, J. (1975). An analysis of tidal strain observations from the United States of America: I. The laterally homogeneous tide. *Bull. Seismol. Soc. Am.* **65,** 1613–1629.

Beavan, J., Evans, K., Mousa, S., and Simpson, D. (1991). Estimating aquifer parameters from analysis of forced fluctuations in well level: An example from the Nubian Formation near Aswan, Egypt 2. Poroelastic properties. *J. Geophys. Res.* **96,** 12139–12160.

Bendat, J. S., and Piersol, A. G. (1986). "Random Data: Analysis and Measurement Procedures." Wiley, New York.

Ben-Zion, Y., Henyey, T. L., Leary, P. C., and Lund, S. P. (1990). Observations and implications of water well and creepmeter anomalies in the Mojave segment of the San Andreas fault zone. *Bull. Seismol. Soc. Am.* **80,** 1661–1676.

Berger, J., and Beaumont, C. (1976). An analysis of tidal strain observations from the United States of America: II. The inhomogeneous tide, *Bull. Seismol. Soc. Am.*, **66,** 1821–1846.

Biot, M. A. (1941). General theory of three-dimensional consolidation, *J. Appl. Phys.* **12,** 155–164.

Biot, M. A. (1956). General solutions of the equations of elasticity and consolidation for a porous material, *J. Appl. Mech.* **23,** 91–96.

Biot, M. A., and Willis, D. G. (1957). The elastic coefficients of the theory of consolidation, *J. Appl. Mech.* **24,** 594–601.

Blanchard, F. B., and Byerly, P. (1935). A study of a well gauge as a seismograph. *Bull. Seismol. Soc. Am.* **25,** 313–321.

Blanpied, M. L., Lockner, D. A., and Byerlee, J. D. (1992). An earthquake mechanism based on rapid sealing of faults. *Nature* **358,** 574–576.

Bodvarsson, G. (1970). Confined fluids as strainmeters. *J. Geophys. Res.* **75,** 2711–2718.

Boehmer, W. K., and Boonstra, J. (1987). Analysis of drawdown in the country rock of composite dike aquifers, *J. Hydrol.* **94,** 199–214.

Boley, B. A., and Weiner, J. H. (1960). "Theory of Thermal Stresses," Wiley, New York.

Booker, J. R. (1974). Time dependent strain following faulting of a porous medium. *J. Geophys. Res.* **79,** 2037–2044.

Boonstra, J., and Boehmer, W. K. (1986). Analysis of data from aquifer and well tests in intrusive dikes, *J. Hydrol.* **88,** 301–317.

Bower, D. R., and Heaton, K. C. (1973). Response of an unconfined aquifer to atmospheric pressure, earth tides and a large earthquake, *In* "Proceedings of the Seventh International Symposium on Earth Tides" (G. Szadeczky-Kardoss, ed.), Akademiai Kiado, Budapest, Hungary, pp. 155–164.

Bower, D. R., and Heaton, K. C. (1978). Response of an aquifer near Ottawa to tidal forcing and the Alaskan earthquake. *Can. J. Earth Sci.* **15,** 331–340.

Bower, D. R. (1983). Bedrock fracture parameters from the interpretation of well tides. *J. Geophys. Res.* **88,** 5025–5035.

Brace, W. F. (1980). Permeability of crystalline and argillaceous rocks. *Int. J. Rock Mech. Min. Sci. Geomech. Abstr.* **17,** 241–251.

Bredehoeft, J. D. (1967). Response of well-aquifer systems to earth tides. *J. Geophys. Res.* **72,** 3075–3087.

Bredehoeft, J. D., Cooper, Jr., H. H., Papadopulos, I. S., and Bennett, R. R. (1965). Seismic fluctuations in an open artesian water well. Geological Survey Research 1965, U.S. Geol. Surv. Prof. Pap. 525-C, pp. 51–57.

Bullen, K. E. (1979). "An Introduction to the Theory of Seismology." 3rd ed. Cambridge University Press, Cambridge.

Byerlee, J. (1990). Friction, overpressure, and fault-normal compression. *Geophys. Res. Lett.* **17,** 2109–2112.

Carrigan, C. R., King, G. C. P., Barr, G. E., and Bixler, N. E. (1991). Potential for water table excursions induced by seismic events at Yucca Mountain, Nevada. *Geology* **19,** 1157–1160.

Clauser, C. (1992). Permeability of crystalline rocks. *EOS, Trans. Am. Geophys. Union* **73,** 233–238.

Cleary, M. P. (1977). Fundamental solutions for a fluid-saturated porous solid. *Int. J. Solids Structures* **13,** 785–806.

Coble, R. W. (1967). The effects of the Alaskan earthquake of March 27, 1964, on ground water in Iowa. *Iowa Acad. Sci. Proc.*, **72,** 323–332.

Cooper, H. H., Jr., Bredehoeft, J. D., Papadopulos, I. S., and Bennett, R. R. (1965). The response of well-aquifer systems to seismic waves. *J. Geophys. Res.* **70,** 3915–3926.

Costain, J. K., Bollinger, G. A., and Speer, J. A. (1987). Hydroseismicity: A hypothesis for the role of water in the generation of intraplate seismicity. *Seismological Res. Lett.* **58,** 41–64.

Davis, G. H., Worts Jr., G. F., and Wilson, Jr., H. D. (1955). Water-level fluctuations in wells. *In* "Earthquakes in Kern County, 1952." Calif. Dept. Nat. Res., Div. Mines Bull. 171, pp. 99–106.

Deng, Q., Jiang, P., Jones, L. M., and Molnar, P. (1981). A preliminary analysis of reported changes in ground water and anomalous animal behavior before the 4 February 1975 Haicheng earthquake. *In* "Earthquake Prediction: An International Review" Maurice Ewing Series 4 (D. W. Simpson, P. G. Richards, eds.), American Geophysical Union, Washington, D.C.

Eaton, J. P., and Takasaki, K. J. (1959). Seismological interpretation of earthquake-induced water-level fluctuations in wells. *Bull. Seismol. Soc. Am.* **49,** 227–245.

Ekstrom, G., Stein, R. S., Eaton, J. P., and Eberhart-Phillips, D. (1992). Seismicity and geometry of a 110-km-long blind thrust fault 1. The 1985 Kettleman Hills, California, earthquake. *J. Geophys. Res.* **97,** 4843–4864.

Evans, K., Beavan, J., and Simpson, D. (1991a). Estimating aquifer parameters from analysis of forced fluctuations in well level: An example from the Nubian Formation near Aswan, Egypt 1. Hydrogeological background and large-scale permeability estimates. *J. Geophys. Res.* **96,** 12127–12137.

Evans, K., Beavan, J., Mousa, S., and Simpson, D. (1991b). Estimating aquifer parameters from analysis of forced fluctuations in well level: An example from the Nubian Formation near Aswan, Egypt 3. Diffusivity estimates for saturated and unsaturated zones. *J. Geophys. Res.* **96,** 12161–12191.

Ewing, W. M., Jardetzky, W. S., and Press, F. (1957). "Elastic Waves in Layered Media." McGraw-Hill, New York.

Fischer, G. J., and Paterson, M. S. (1992). Measurement of permeability and storage capacity in rocks during deformation at high temperature and pressure. Chapter 9 in "Fault Mechanics and Transport Properties of Rocks." Academic Press, New York.

Fletcher, J. B., and Sykes, L. R. (1977). Earthquakes related to hydraulic mining and natural seismic activity in western New York state. *J. Geophys. Res.* **82,** 3767–3780.

Freeze, R. A., and Cherry, J. A. (1979). "Groundwater." Prentice-Hall, New Jersey.

Galloway, D. L., and Wilcoxon, W. C. (1993). Earth-tide induced fluid pressure changes in Devils Hole, Death Valley National Monument, California–Nevada. *EOS, Trans. Am. Geophys. Union* **74,** 565.

Godin, G. (1972). "The Analysis of Tides." University of Toronto Press, Toronto.

Green, D. H., and Wang, H. F. (1986). Fluid pressure response to undrained compression in saturated sedimentary rock. *Geophysics* **51,** 948–956.

Green, D. H., and Wang, H. F. (1990). Specific storage as a poroelastic coefficient. *Water Resources Res.* **26,** 1631–1637.

Hanson, J. M., and Owen, L. B. (1982). Fracture orientation analysis by the solid earth tidal strain method. Paper presented at 57th Annual Fall Technical Conference and Exhibition of the Society of Petroleum Engineers of AIME, New Orleans, LA, Sept. 26–29, 1982.

Harrison, J. C. (1971). "New Computer Programs for the Calculation of Earth Tides." Report of the Cooperative Institute for Research in Environmental Sciences, University of Colorado, Boulder.

Headworth, H. G., Keating, T., and Packman, M. J. (1982). Evidence for shallow highly-permeable zone in the Chalk of Hampshire, U.K. *J. Hydrol.* **55,** 93–112.

Hill, D. P., Reasenberg, P. A., Michael, A., Arabasz, W. J., Beroza, G., Brumbaugh, D., Brune, J. N., Castro, R., Davis, S., dePolo, D., Ellsworth, W. L., Gomberg, J., Harmsen, S., House, L., Jackson, S. M., Johnston, M. J. S., Jones, L., Keller, R., Malone, S., Munguia, L., Nava, S., Pechman, J. C., Sanford, A., Simpson, R. W., Smith, R. B., Stark, M., Stickney, M., Vidal, A., Walter, S., Wong, V., and Zollweg, J. (1993). Seismicity remotely triggered by the magnitude 7.3 Landers, California, earthquake. *Science* **260,** 1617–1623.

Hsieh, P. A., and Bredehoeft, J. D. (1981). A reservoir analysis of the Denver earthquakes: A case of induced seismicity, *J. Geophys. Res.* **86,** 903–920.

Hsieh, P. A., Bredehoeft, J. D., and Farr, J. M. (1987). Determination of aquifer transmissivity from earth-tide analysis. *Water Resources. Res.* **78,** 1824–1832.

Hudnut, K. W., Seeber, L., and Pacheco, J. (1989). Cross-fault triggering in the November 1987 Superstition Hills earthquake sequence, southern California. *Geophys. Res. Lett.* **16,** 199–202.

Jaumé, S. C., and Sykes, L. R. (1992). Changes in state of stress on the southern San Andreas fault resulting from the California earthquake sequence of April to June, 1992. *Science* **258,** 1325–1328.

Johnson, A. G., Kovach, R. L., Nur, A., and Booker, J. R. (1973). Pore pressure changes during creep events on the San Andreas fault, *J. Geophys. Res.* **78,** 851–857.

Kawabe, I., Ohno, I., and Nadano, S. (1988). Groundwater flow records indicating earthquake occurrence and induced earth's free oscillations. *Geophys. Res. Lett.* **15,** 1235–1238.

Keller, C. K., van der Kamp, G., and Cherry, J. A. (1989). A multiscale study of the permeability of a thick clayey till. *Water Resources Res.* **25,** 2299–2317.

Li, V. C. (1984/85). Estimation of in-situ hydraulic diffusivity of rock masses. *Pure Appl. Geophys.* **122,** 546–559.

Lippincott, D. K., Bredehoeft, J. D., and Moyle, Jr., W. R. (1985). Recent movements on the Garlock fault as suggested by water-level fluctuations in a well in Fremont Valley, California. *J. Geophys. Res.* **90,** 1911–1924.

Liu, L. B., Roeloffs, E., and Zheng, X. Y. (1989). Seismically induced water level oscillations in the Wali well, Beijing, China. *J. Geophys. Res.* **94,** 9453–9462.

Ma, Z.-J., Fu, Z.-X., Zhang, Y.-Z., Wang, C.-M., Zhang, G.-M., and Liu, D.-F. (1989). "Earthquake Prediction: Nine Major Earthquakes in China (1966–1976)." Seismological Press, Springer-Verlag, Beijing.

Maslia, M. L., and Prowell, D. C. (1990). Effect of faults on fluid flow and chloride contamination in a carbonate aquifer system. *J. Hydrol.* **115,** 1–49.

McPherson, R. C., and Dengler, L. A. (1992). The Honeydew earthquake. *California Geology* **45,** 31–39.

Mesri, G., Adachi, K., and Ullrich, C. R. (1976). Pore–pressure response in rock to undrained change in all-round stress. *Geotechnique* **26,** 317–330.

Morin, R. H., and Olsen, H. W. (1987). Theoretical analysis of the transient pressure response from a constant flow rate hydraulic conductivity test. *Water Resources Res.* **23,** 1461–1470.

Muir-Wood, R., and King, G. C. P. (1993). Hydrological signatures of earthquake strain. *J. Geophys. Res.* **98,** 22035–22068.

Narasimhan, T. N., Kanehiro, B. Y., and Witherspoon, P. A. (1984). Interpretation of earth tide response of three deep, confined aquifers, *J. Geophys. Res.* **89,** 1913–1924.

Nativ, R., and Gutierrez, G. N. (1989). Hydrogeology and hydrochemistry of Cretaceous aquifers, Southern High Plains, U.S.A. *J. Hydrol.* **108,** 79–109.

Neuzil, C. E. (1986). Groundwater flow in low-permeability environments. *Water Resources Res.* **22,** 1163–1195.

Nicholson, C., Roeloffs, E., and Wesson, R. L. (1988). The northeastern Ohio earthquake of 31 January 1986: Was it induced? *Bull. Seismol. Soc. Am.* **78,** 188–217.

Nur, A., and Booker, J. R. (1972). Aftershocks caused by pore fluid flow? *Science* **175,** 885.

Okada, Y. (1992). Internal deformation due to shear and tensile faults in a half-space. *Bull. Seismol. Soc. Am.* **82,** 1018–1040.

Oliver, J. (1962). A summary of observed seismic surface wave dispersions. *Bull. Seismol. Soc. Am.* **52,** 81–86.

Pickens, J. F., Grisak, G. E., Avis, J. D., Belanger, D. W., and Thury, M. (1987). Analysis and interpretation of borehole hydraulic tests in deep boreholes: Principles, model development, and application. *Water Resources Res.* **23,** 1341–1375.

Quilty, E. G., and Roeloffs, E. (1991). Removal of barometric pressure response from water level data. *J. Geophys. Res.* **96,** 10209–10218.

Rasheeduddin, M., Yazicigil, H., and Al-Layla, R. I. (1989). Numerical modeling of a multiaquifer system in eastern Saudi Arabia, *J. Hydrol.* **107,** 193–222.

Rexin, E. E., Oliver, J., and Prentiss, D. (1962). Seismically-induced fluctuations of the water level in the Nunn-Bush well in Milwaukee. *Bull. Seismol. Soc. Am.* **52,** 17–25.

Rice, J. R. (1992). Fault stress states, pore pressure distributions, and the weakness of the San Andreas fault. *In* "Fault Mechanics and the Transport Properties of Rocks" (B. Evans, T.-F. Wong, eds.). Academic Press, San Diego.

Rice, J. R., and Cleary, M. P. (1976). Some basic stress diffusion solutions for fluid-saturated elastic porous media with compressible constituents. *Revs. Geophys. Space Phys.*, **14,** 227–241.

Rice, J. R., and Simons, D. A. (1976). The stabilization of spreading shear faults by coupled deformation-diffusion effects in fluid-infiltrated porous materials. *J. Geophys. Res.* **81,** 5322–5344.

Ritzi, Jr., R. W., Sorooshian, S., and Hsieh, P. A. (1991). The estimation of fluid flow properties from the response of water levels in wells to the combined atmospheric and earth tide forces, *Water Resources Res.* **27,** 883–893.

Roeloffs, E. (1988a). Fault stability changes induced beneath a reservoir with cyclic variations in water level. *J. Geophys. Res.* **93,** 2107–2124.

Roeloffs, E. (1988b). Hydrologic precursors to earthquakes: A review. *Pure Appl. Geophys.* **126,** 177–209.

Roeloffs, E. (1993). A reported streamflow increase. *In* "The Loma Prieta, California, Earthquake of October 17, 1989—Preseismic Observations" (M. Johnston, ed.). U.S. Geological Survey Professional Paper 1550-C.

Roeloffs, E., Danskin, W., Farrar, C., Galloway, D. L., Hamlin, S., Quilty, E. G., Quinn, H. M., Schaefer, D. H., Sorey, M., and Woodcock, D. (1995). Hydrologic effects of the June 28, 1992 Landers, California, earthquake. U.S. Geological Survey Open-File Report 95-42.

Roeloffs, E., and Quilty, E. G. (1995). Water level and strain changes preceding and following the August 4, 1985 Kettleman Hills, California, earthquake. *Pure Appl. Geophys.* (in press).

Roeloffs, E., and Rudnicki, J. W. (1984/85). Coupled deformation-diffusion effects on water-level changes due to propagating creep events, *Pure and Appl. Geophys.* **122,** 560–582.

Roeloffs, E., Schulz-Burford, S., Riley, F. S., and Records, A. W. (1989). Hydrologic effects on water level changes associated with episodic fault creep near Parkfield, California. *J. Geophys. Res.* **94,** 12387–12402.

Rojstaczer, S. (1987). The local effects of groundwater pumpage within a fault-influenced groundwater basin, Ash Meadows, Nye County, Nevada, U.S.A. *J. Hydrol.* **91,** 319–337.

Rojstaczer, S. A. (1988a). Determination of fluid flow properties from the response of water levels in wells to atmospheric loading. *Water Resources Res.* **24,** 1927–1938.

Rojstaczer, S. A. (1988b). Intermediate period response of water levels in wells to crustal strain: Sensitivity and noise level. *J. Geophys. Res.* **93,** 13619–13634.

Rojstaczer, S. A., and Riley, F. S. (1990). The response of the water level in a well to earth tides and atmospheric loading under unconfined conditions. *Water Resources. Res.* **26,** 1803–1817.

Rojstaczer, S., and Wolf, S. (1992). Permeability changes associated with large earthquakes: An example from Loma Prieta, California, 10/17/89. *Geology* **20,** 211–214.

Roth, P., Pavoni, N., and Deichmann, N. (1992). Seismotectonics of the eastern Swiss Alps and evidence for precipitation-induced variations of seismic activity. *Tectonophysics* **207,** 183–197.

Rudnicki, J. W. (1986). Slip on an impermeable plane in a fluid-saturated rock mass. *In* "Earthquake Source Mechanics." Geophysical Monograph 37 (Maurice Ewing 6), American Geophysical Union, Washington, DC.

Rudnicki, J. W. (1987). Plane strain dislocations in linear elastic diffusive solids. *J. Appl. Mech.* **109,** 545–552.

Rudnicki, J. W., and Hsu, T. C. (1988). Pore pressure changes induced by slip on permeable and impermeable faults. *J. Geophys. Res.* **93,** 3275–3285.

Rudnicki, J. W., and Koutsibelas, D. A. (1991). Steady propagation of plane strain shear cracks on an impermeable plane in an elastic diffusive solid. *Int. J. Solids Structures* **27,** 205–225.

Rudnicki, J. W., and Roeloffs, E. A. (1990). Plane-strain shear dislocations moving steadily in linear elastic diffusive solids. *J. Appl. Mech.—Trans. A.S.M.E.* **57,** 32–39.

Rudnicki, J. W., Yin, J., and Roeloffs, E. A. (1993). Analysis of water level changes induced by fault creep at Parkfield, California. *J. Geophys. Res.* **98,** 8143–8152.

Rushton, K. R., and Weller, J. (1985). Response to pumping of a weathered-fractured granite aquifer. *J. Hydrol.* **80,** 299–309.

Scholz, C. H. (1990). "The Mechanics of Earthquakes and Faulting." Cambridge University Press, Cambridge, U.K.

Scott, J. S., and Render, F. W. (1964). Effect of an Alaskan earthquake on water levels in wells in Winnipeg and Ottawa. *J. Hydrol.* **2,** 262–268.

Segall, P. (1989). Earthquakes triggered by fluid extraction. *Geology* **17,** 942–946.

Segall, P. (1992). Induced stresses due to fluid extraction from axisymmetric reservoirs. *Pure Appl. Geophys.* **139,** 535–560.

Sibson, R. H. (1990). Rupture nucleation on unfavorably oriented faults. *Bull. Seismol. Soc. Am.* **80,** 1580–1604.

Sibson, R. H. (1992). Implications of fault-valve behavior for rupture nucleation and recurrence. *Tectonophysics* **211,** 283.

Stein, R. S., King, G. C. P., and Lin, J. (1992). Changes in failure stress on the southern San Andreas fault system caused by the 1992 magnitude = 7.4 Landers earthquake. *Science* **258,** 1328–1332.

Subyani, A. M., and Sen, Z. (1989). Geostatistical modeling of the Wasia aquifer in central Saudi Arabia. *J. Hydrol.* **110,** 295–314.

Talwani, P., and Acree, S. (1984/85). Pore pressure diffusion and the mechanism of reservoir induced seismicity. *Pure Appl. Geophys.* **122,** 947–965.

Versey, H. R., and Singh, B. K. (1982). Groundwater in Deccan basalts of the Betwa Basin, India. *J. Hydrol.* **58,** 279–306.

Wakita, H. (1975). Water wells as possible indicators of tectonic strain. *Science* **189,** 553–555.

Waller, R. M., Thomas, H. E., and Vorhis, R. C. (1965). Effects of the Good Friday earthquake on water supplies. *J. Amer. Water Works Assoc.* **57,** 123–131.

Wang, C.-M., Wang, Y.-L., Zhang, H.-P., Li, Y., and Zhao, S. (1979). Characteristics of water level variations in deep wells before and after the Tangshan earthquake of 1976. *In* "Earthquake Prediction." Proceedings of the International (UNESCO) Symposium on Earthquake Prediction, Paris, France, 1979.

Wang, H. F. (1993). Quasi-static poroelastic parameters in rock and their geophysical applications. *Pure Appl. Geophys.* **141,** 269–286.

Weeks, E. P. (1979). Barometric fluctuations in wells tapping deep unconfined aquifers. *Water Resources Res.* **15,** 1167–1176.

Weertman, J. (1974). Water flow paths around a dislocation on an earthquake fault. *J. Geophys. Res.* **79,** 3291–3293.

Wei, H. F., Ledoux, E., and de Marsily, G. (1990). Regional modeling of groundwater flow and salt and environmental tracer transport in deep aquifers in the Paris Basin. *J. Hydrol.* **120,** 341–358.

Whitehead, R. L., Harper, R. W., and Sisco, H. G. (1984/85). Hydrologic changes associated with the October 28, 1983, Idaho earthquake. *Pure Appl. Geophys.* **122,** 280–293.

Wood, S. H. (1985). Regional increase in groundwater discharge after the 1983 Idaho earthquake: Coseismic strain release, tectonic, and natural hydraulic fracturing. *In* "Proceedings of Workshop XXVIII on the Borah Peak, Idaho, Earthquake," Vol. A (R. S. Stein and R. C. Bucknam, eds.). U.S. Geological Survey Open-File Report 85–290.

Wu, F. T., Han, D., and Zheng, Z. (1984). Filtration of short baseline and water level data before and after the Tangshan earthquake. *In* "A Collection of Papers of the International Symposium on Continental Seismicity and Earthquake Prediction." Seismological Press, Beijing, China, pp. 549–570.

Zhang, G.-M., and Qiou, J.-N. (1979). An analysis of the process of preparation and the medium-term precursors of the 1976 Tangshan earthquake. *In* "Earthquake Prediction." Proceedings of the International (UNESCO) Symposium on Earthquake Prediction, Paris, France, 1979.

Zhu, F. M., and Zhong, Y.-Z (1979). Anomalous macroscopic phenomena and their significance in the prediction of strong earthquakes. *In* "Earthquake Prediction." Proceedings of the International (UNESCO) Symposium on Earthquake Prediction, Paris, France, 1979.

Zoback, M. D., Zoback, M. L., Mount, V. S., Suppe, J., Eaton, J. P., Healy, J. H., Oppenheimer, D., Reasenberg, P., Jones, L., Raleigh, C. B., Wong, I. G., Scotti, O., and Wentworth, C. (1987). New evidence on the state of stress of the San Andreas fault system, *Science* **238,** 1105–1111.